From the Department of Molecular Medicine and Surgery
Karolinska Institutet, Stockholm, Sweden

MYOCARDIAL HYPERTROPHY AND EXTRACELLULAR VOLUME BY CARDIOVASCULAR MAGNETIC RESONANCE IMAGING

Magnus Lundin

Karolinska Institutet

Stockholm 2020

Published by Karolinska Institutet.
Printed by Universitetsservice US-AB.

ISBN 978-91-7831-850-6

MYOCARDIAL HYPERTROPHY AND EXTRA-CELLULAR VOLUME BY CARDIOVASCULAR MAGNETIC RESONANCE IMAGING
THESIS FOR DOCTORAL DEGREE (Ph.D.)

By

Magnus Lundin

Principal Supervisor:
Martin Ugander
Karolinska Institutet
Department of Molecular Medicine and Surgery
Division of Clinical Physiology

Co-supervisor(s):
Andreas Sigfridsson
Karolinska Institutet
Department of Molecular Medicine and Surgery
Division of Clinical Physiology

Kenneth Caidahl
Karolinska Institutet
Department of Molecular Medicine and Surgery
Division of Clinical Physiology

Opponent:
Marc Dweck
University of Edinburgh
Centre for Cardiovascular Science

Examination Board:
Thomas Gustafsson
Karolinska Institutet
Department of Laboratory Medicine
Division of Clinical Physiology

Tomas Bjerner
Uppsala University
Department of Surgical Sciences
Division of Radiology

Agnes Modin
Karolinska Institutet
Department of Molecular Medicine and Surgery
Division of Clinical Physiology

To Anita and Ingemar.

ABSTRACT

Cardiovascular disease contributes greatly to the disease burden in many developed countries. Cardiovascular magnetic resonance (CMR) is a powerful imaging modality that can diagnose a vast range of these diseases. When combined with an extracellular contrast agent, CMR can not only diagnose the function and size of the heart but also provide detailed information on the myocardial tissue. CMR T_1 and extracellular volume (ECV) mapping can be used to quantitatively characterise the tissue properties of the myocardium. The main objective of this work was to determine how to use these and other imaging capabilities of CMR imaging in order to maximise the diagnostic abilities and predict adverse outcomes.

Study I examined whether T_1 and ECV mapping could be useful for detecting myocarditis when acquired early after contrast administration. *Study II* looked at the prevalence of diffusely increased ECV in a clinical population. *Study III* presents a novel way of calculating global wall thickness (GT), *i e* the average thickness of the whole left ventricle. GT can easily be calculated from the left ventricular mass and volume which are measured as a part of a normal CMR examination. *Study IV* examined the feasibility of determining the myocardial cell size using early T_1 mapping and calculating the intra-cellular lifetime of water (tau).

Study I found no benefit of performing early compared to late post-contrast imaging when detecting myocarditis. *Study II* found that found that 8 % of a clinical population had diffusely increased ECV, that increased ECV was more common in patients with a dilated left ventricle and that focal lesions were more common in patients with decreased systolic function. *Study III* derived and validated a new measure for global wall thickness (GT) that can be easily calculated from the left ventricular mass (LVM) and volume. GT was highly prognostic in patients with otherwise normal findings and can be used together with LVM to classify different types of hypertrophy. *Study IV* found that measuring the size of cardiomyocytes using contrast-enhanced CMR in a clinical setting was not reliable using the slow exchange model of transcytolemmal water exchange.

LIST OF SCIENTIFIC PAPERS

I. **Magnus Lundin**, Peder Sörensson, Liya Vishneskaya, Eva Maret, Peter Kellman, Andreas Sigfridsson, Martin Ugander.
Detection of myocarditis using T1- and ECV mapping is not improved by early compared to late postcontrast imaging
Clin Physiol Funct Imaging. 2019 Nov;39(6):384-392.

II. **Magnus Lundin**, Peder Sörensson, Eva Maret, Jonas Jenner, Goran Abdula, Jannike Nickander, Raquel Themudo, Kenneth Caidahl, Peter Kellman, Andreas Sigfridsson, Martin Ugander.
Diffusely increased myocardial extracellular volume with or without focal late gadolinium enhancement – prevalence and associations with left ventricular size and function
J Thorac Imaging. 2020 Apr 7. [Epub ahead of print]

III. **Magnus lundin**, Einar Heiberg, David Nordlund, Tom Gyllenhammar, Katarina Steding-Ehrenborg, Henrik Engblom, Marcus Carlsson, Dan Atar, Jesper van der Pals, David Erlinge, Rasmus Borgquist, Ardavan Khoshnood, Ulf Ekelund, Jannike Nickander, Raquel Themudo, Sabrina Nordin, Rebecca Kozor, Anish N Bhuva, James C Moon MBBCh, Eva Maret, Kenneth Caidahl, Andreas Sigfridsson, Peder Sörensson, Erik B Schelbert, Håkan Arheden, Martin Ugander.
Left ventricular mass and global wall thickness – prognostic utility and characterization of left ventricular hypertrophy
Submitted

IV. **Magnus Lundin**, Peder Sörensson, Eva Maret, Peter Kellman, Andreas Sigfridsson, Martin Ugander.
Indirect measurement of cardiomyocyte size by contrast-enhanced cardiovascular magnetic resonance imaging—a clinical feasibility study at 1.5T
Manuscript

CONTENTS

LIST OF ABBREVIATIONS

BSA	Body surface area
CMR	Cardiovascular magnetic resonance
CRT	Cardiac resynchronization therapy
ECV	Extracellular volume
EGE	Early gadolinium enhancement
EMB	Endomyocardial biopsy
EVF	Erythrocyte volume fraction
GBCA	Gadolinium-based contrast agents
GRE	Global relative enhancement
GT(i)	Global wall thickness (indexed to BSA)
HCM	Hypertrophic cardiomyopathy
hct	Haematocrit
HHF	Hospitalisation for heart failure
KAMRAT	*KArolinska universitetssjukhusets studie av Magnetisk Resonanstomografi av hjärtat*
LGE	Late gadolinium enhancement
LV	Left ventricular
LVEDV(i)	Left ventricular end-diastolic volume (indexed to BSA)
LVEF	Left ventricular ejection fraction
LVH	Left ventricular hypertrophy
LVM(i)	Left ventricular mass (indexed to BSA)
MOLLI	Modified Look-Locker inversion recovery
MRI	Magnetic resonance imaging
NMR	Nuclear magnetic resonance
NSF	Nephrogenic systemic fibrosis
PSIR	Phase-sensitive inversion recovery
RF	Radio frequency
ROI	Region of interest
RWT	Relative wall thickness
SASHA	Saturation recovery single shot acquisition
ShMOLLI	Shortened MOLLI
SI	Signal intensity
SSFP	Steady state free precession
TI	Inversion time

1 CARDIAC MAGNETIC RESONANCE IMAGING

1.1 MAGNETIC RESONANCE IMAGING (MRI)

Magnetic resonance imaging (MRI) is an imaging methodology based on the nuclear magnetic resonance (NMR) method. Spin is a form of angular momentum in atomic nuclei and other particles. Both neutrons and protons have non-zero spin and NMR is only feasible on isotopes that have an odd number of neutrons and/or protons. Particles with non-zero spin also have a non-zero magnetic dipole moment. When this magnetic dipole moment is exposed to an external magnetic field, its corresponding angular momentum vector will start rotating, a process called precession. The angular momentum vector will precess at the Larmor frequency *f,* which is determined by the gyromagnetic ratio γ and the magnetic field strength *B* as.

$$f = \frac{\gamma}{2\pi} B \quad \text{(Equation 1)}$$

When considering an ensemble of many particles exposed to a magnetic field, the particles' angular momentum vectors will start to precess and they will have a slight tendency to precess around an axle parallel to the magnetic field causing slightly more magnetisation in this direction. It is this small net magnetisation vector that makes MRI possible (1).

The magnetic field strength is measured in Tesla (T) and the most commonly used field strengths of MRI scanners in clinical settings are 1.5 T and 3 T. Higher field strengths will have larger net magnetisation vectors but higher field strength is not always desirable, not least due to cost.

In medical imaging, hydrogen is the most commonly imaged isotope due to its abundance in the body as part of water molecules. For hydrogen the gyromagnetic ratio $\gamma/(2\pi)$ is approximately 42.6 MHz/T and from Equation 1 follows that the Larmor frequency for hydrogen is 64 MHz and 128 MHz at 1.5 T and 3 T respectively. Since these frequencies are close to the commercial radio frequency band (88–108 MHz), shielding the MRI scanner from outside interference is essential.

1.2 T_1 AND T_2

The precession in the magnetic field does not generate any signal in its equilibrium state unless there is a disturbance. This disturbance is caused by the radio frequency (RF) transmitter coils of the scanner emitting RF pulses tuned to Larmor frequency. The RF pulse needs to be perpendicular to the magnetic field and generates both an electrical field and a magnetic field. When trying to adapt to the new magnetic field, the net magnetisation vector deviates from its equilibrium position.

Following the RF pulse, the net magnetisation vector will return to its original state. During this process, further RF pulses can be applied in order to perform a readout. The readout pulse turns the net magnetisation vector slightly, and this generates a signal perpendicular to

the magnetic field during this readout phase that can be detected by RF receiver coils tuned to the same frequency as the transmitter coils. Since the signal is comparatively weak, these coils need to be placed in close proximity to the imaged object, which often means being placed close to the patient's body.

The return to the equilibrium state is described by two time constants: T_1 or spin-lattice relaxation time, and T_2 or spin-spin relaxation time. T_2 describes how long time it takes for the magnetisation to disperse in the horizontal plane (*xy*-plane) perpendicular to the magnetic field (in the *z*-direction), and T_1 how long time it takes for the signal to recover in the (*z*) direction of the magnetic field. These recoveries are described by the following two equations and figures:

$$M_z = M_0(1 - e^{-\frac{t}{T_1}}) \quad \text{(Equation 2)}$$

$$M_{xy} = M_0\, e^{-\frac{t}{T_2}} \quad \text{(Equation 3)}$$

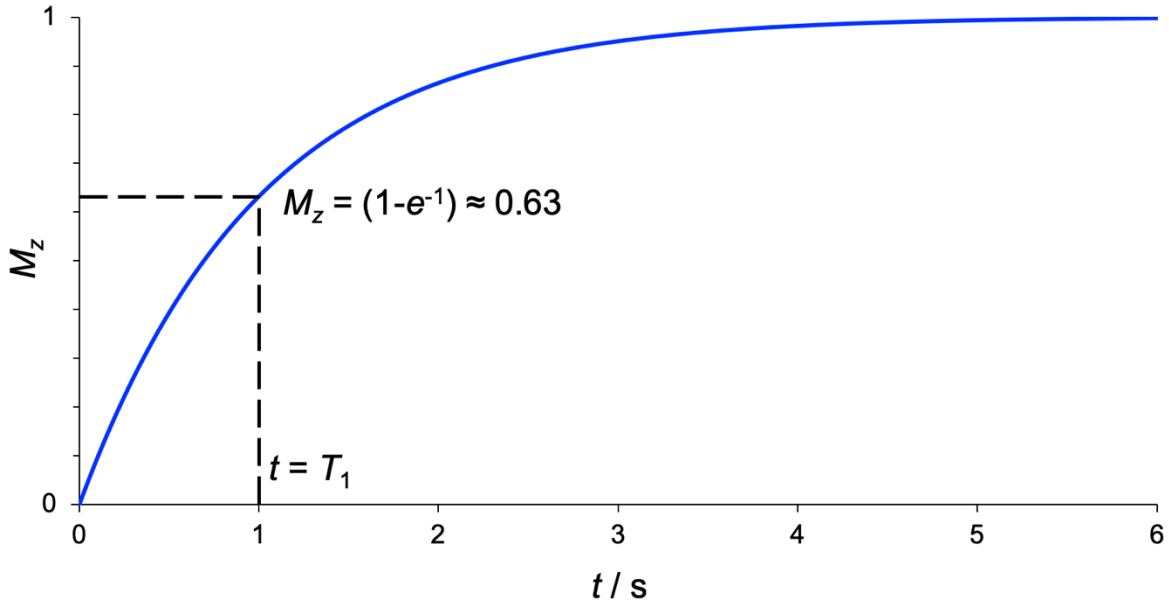

Figure 1. T_1 relaxation
This figure shows an example of T_1 relaxation with the signal recovering in the (*z*) direction of the magnetic field at a rate determined by T_1 as described in Equation 2. In this example T_1 is 1 s which is a normal value for native T_1 in myocardium.

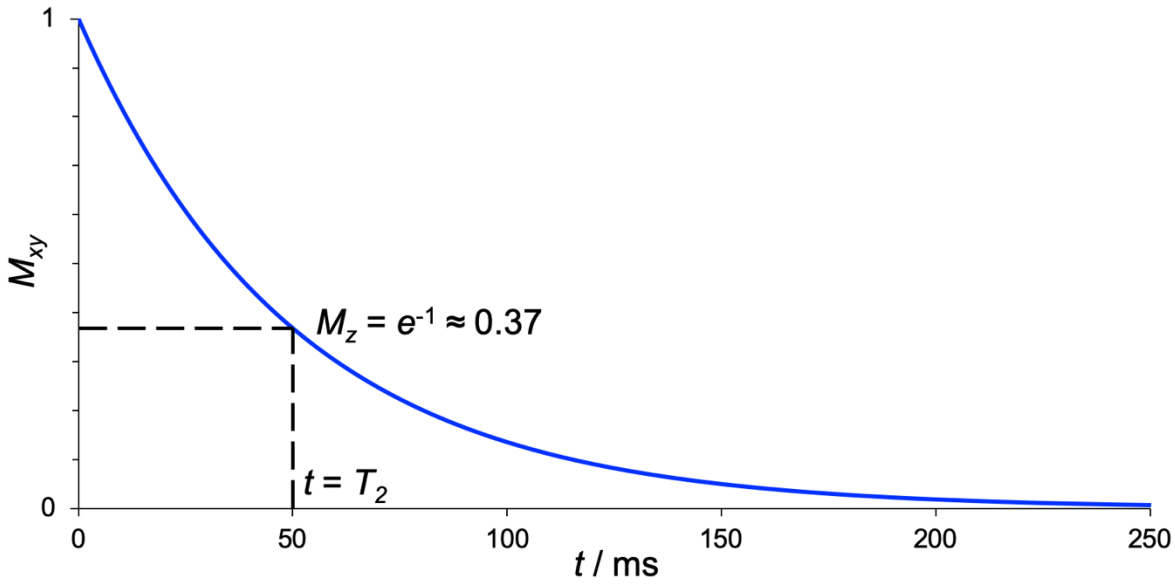

Figure 2. T_2 relaxation
This figure shows an example of T_2 relaxation with the signal disappearing in the (xy) plane, perpendicular to the magnetic field at a rate determined by T_2 as described in Equation 3. In this example T_2 is 50 ms which is a normal value for T_2 in myocardium.

1.3 T_1 MAPPING

Early work on T_1 measurement was performed by Look and Locker in the late 1960's for application in nuclear magnetic resonance spectroscopy (2,3). It took several decades before a T_1 mapping could be applied clinically in CMR, and this sequence was called the modified Look-Locker inversion recovery (MOLLI) sequence (4), which was found to provide reproducible T_1 values (5). In MOLLI, the magnetisation is flipped 180º and the return to the original state, which is governed by T_1, is measured by exposing the recovering signal for small disturbances, flipping the signal by a certain number of degrees in order to obtain a signal in the xy-plane that is measurable.

An issue when doing an inversion (180° pulse) followed by successive readouts is that the signal will be affected by the readouts. This means that T_1* is measured and not the actual T_1. Consequently, T_1 has to be obtained using a correction factor which is only valid for small flip angles (6) and inadequate correction can cause errors. The difference between the undisturbed T_1 relaxation and the relaxation affected by repeated readouts is shown in Figure 3.

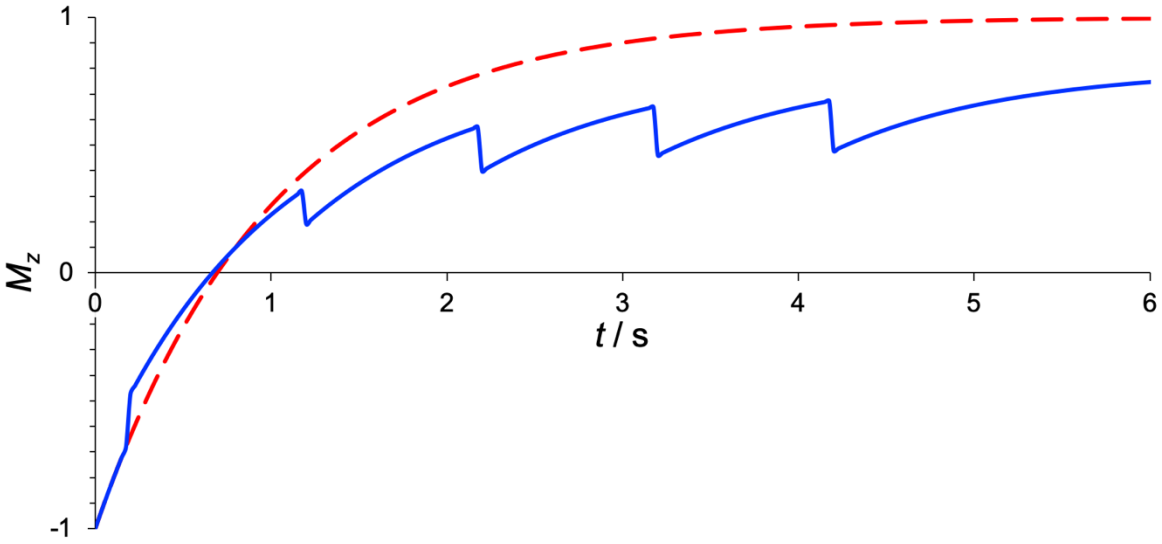

Figure 3. T_1 relaxation with and without readouts.
This figure shows T_1 relaxation which is affected by readouts every second (blue solid line) and T_1 relaxation that is not affected but any readouts (dashed red line). In this example T_1 is again set to 1 s for both curves.

The original MOLLI sequence used three inversions followed by read-outs at end diastole in the following pattern: first inversion followed by three read-outs, (and three heartbeats pause); second inversion followed by three read-outs (and three heartbeats pause); third inversion followed by five readouts (4). This original MOLLI was therefore called 3(3)3(3)5, and encompassed 17 heartbeats in total. The pauses are needed for full relaxation, normally 5 times T_1 is considered enough to allow for adequate relaxation, but this has to be increased to even longer times when readouts are performed, as evident in Figure 3.

Although the original 17 heartbeat MOLLI could be performed within one breath-hold, some patients would struggle with such a duration of breath-hold. This was later shortened to two inversions and eleven heartbeats 3(3)5 (7) which was found to give similar results for T_1 (8) and changed to 5(3)3 in order to reduce heart rate dependency (9). Three inversions but fewer readouts in the form om 4(1)3(1)2 was found to be superior for lower values of T_1 which occur post-contrast. The latter two MOLLI-versions were later modified to count seconds instead of heartbeats, *i e* readouts during at least five seconds followed by at least three seconds pause, etc, in order to make time for sufficient signal relaxation. These versions were called 5s(3s)3s and 4s(1s)3s(1s)2s and only differ for heartrates above 60 beats per minute.

Other versions of T_1 mapping have also been described. One of these is called Shortened MOLLI (ShMOLLI) which only uses 9 heartbeats 5(1)1(1)1 and is less heartrate dependent than the original MOLLI (10). An alternative to performing T_1 mapping using inversion recovery is to use saturation recovery such as SAturation recovery Single Shot Acquisition (SASHA) (11). SASHA saturates the signal with the benefit that for each readout, the readout does not affect future readouts in the way that happens with MOLLI. However, the drawback with SASHA is that the dynamic range is half as large (0 to 1 instead of -1 to 1 for MOLLI).

This results in SASHA having a better accuracy but worse precision compared to MOLLI (12), *i e* on average the results will be more correct but the variability will be higher. The studies that form part of this thesis mainly use the 5(3)3 version of MOLLI for both pre- and post-contrast T_1 mapping.

1.4 ECV MAPPING

The inverse of T_1 is called the relaxation rate, R_1, and the difference in R_1 between post- and pre-contrast images is called ΔR_1, which is proportional to the concentration of contrast agent, according to the following equation.

$$\frac{1}{T_{1,\ \text{post-contrast}}} - \frac{1}{T_{1,\ \text{pre-contrast}}} = R_{1,\ \text{post-contrast}} - R_{1,\ \text{pre-contrast}=} =$$
$$\Delta R_1 \sim \text{contrast agent concentration} \quad \text{(Equation 4)}$$

Since ΔR_1 is proportional to contrast agent concentration, the contrast agent's partition coefficient λ between the tissue and the blood pool can be calculated from T_1 measured in the myocardium and blood pool respectively as:

$$\lambda = \frac{\Delta R_{1\ \text{myocardium}}}{\Delta R_{1\ \text{blood}}} \quad \text{(Equation 5)}$$

If the contrast agent is extracellular in its biodistribution, which most contrast agents are, the extracellular volume (ECV) fraction of the myocardium can be calculated if the ECV of blood is known. In a centrifuged blood sample, the red blood cells (erythrocytes) will end up at the bottom of the tube and their proportion of the sample is called haematocrit (hct) or erythrocyte volume fraction (EVF). The ECV of the blood sample is therefore the remaining part of the blood sample calculated as (1-hct). The myocardial ECV can thus be calculated as:

$$ECV_{myoardium} = \frac{\Delta R_{1\ myocardium} \cdot (1-hct)}{\Delta R_{1\ blood}} \quad \text{(Equation 6)}$$

Early work on distribution volumes was performed as early as in the late 1990's when the distribution volume of gadopentetate dimeglumine was compared to that of 99mTc-DTPA using magnetic resonance imaging and autoradiography respectively. These methods were found to provide similar results, and the distribution volume was the extracellular space which also was found to be increased in reperfused infarction (13). With the advent of T_1 mapping it was not only possible to measure ECV in an area but also on a pixel by pixel basis (7), which was additionally made easier by implementing automated motion correction and co-registration (14).

1.5 CONTRAST AGENTS

To increase the sensitivity of magnetic resonance imaging, contrast agents can be used. These can be ferromagnetic, paramagnetic, or superparamagnetic and they affect T_1 as well as T_2. Ferromagnetic contrast agents contain iron and mainly affect T_2, while the most commonly used contrast agents contain gadolinium (Gd), and gadolinium-based contrast agents (GBCA)

mainly affect T_1. GBCA are indirect contrast agents since their effect is shortening of the relaxation times of the water protons in their immediate vicinity. The water protons' T_1 is shortened, and this causes increased signal intensity (15).

In contrast agents, Gd is always bound to a carrier molecule, or chelate. The dissociated non-chelated Gd (Gd^{3+}) can be deposited in various parts of the body and have toxic effects at concentrations that are rarely achieved clinically (16). The compound structure of GBCA can either be linear or macrocyclic where the macrocyclic types tend to be more stable with lower risk of dissociation and therefore safer (16). There are both ionic and non-ionic GBCA, where the ionic agents tend be more stable (17). In the studies that are part of this thesis, only macrocyclic contrast agents were used, both ionic and non-ionic.

Immediate adverse reactions are rare and serious reactions even more so with 614 reported severe reactions in 200 million administrations of GBCA, equating to one severe reaction for 325 000 exams (17). The effects of GBCA on the foetus or child in pregnant or lactating women are poorly known and contrast administration is therefore only performed on a case-by-case basis according to most guidelines (17).

In 2006, several cases of nephrogenic systemic fibrosis (NSF) were found in patients with end-stage renal disease that were on dialysis and that had undergone MRI with GBCA (18). The half-life to renal excretion for GBCA is roughly two hours in patients with normal renal function, but this time is greatly increased in patients with severely impaired renal function. This gives increased time for the Gd ions to be dissociated from their chelates, form complexes in tissue which leads to a response from the immune system which in turn leads to fibrosis (17). Macrocyclic GBCA account for less than 1 % of the cases of NSF due to their higher stability (17). Early work on contrast-enhanced CMR was done using a gadolinium (Gd) molecule coupled with diethylenetriaminepentaacetic acid (DTPA) (19), and the versions of GBCA with Gd-DTPA make up the overwhelming majority of NSF cases (17).

1.6 LATE GADOLINIUM ENHANCEMENT (LGE)

Late gadolinium enhancement (LGE) is the standard technique for identifying focal lesions in the myocardium of both ischemic (20) and non-ischemic (21) origin. The extracellular contrast agents distribute into the extracellular space, which will be expanded in the setting of myocardial necrosis and fibrosis. The LGE sequence is similar to the MOLLI sequence inasmuch both are inversion recovery sequences. The focal areas with an expanded extracellular space will have a lower T_1 due to the increased relative contrast agent concentration, and will therefore recover faster compared to normal tissue (22). When performing LGE imaging, an inversion time (TI) needs to bet set while scanning, to null the signal of presumably healthy myocardium, which provides maximum contrast, see Figure 4.

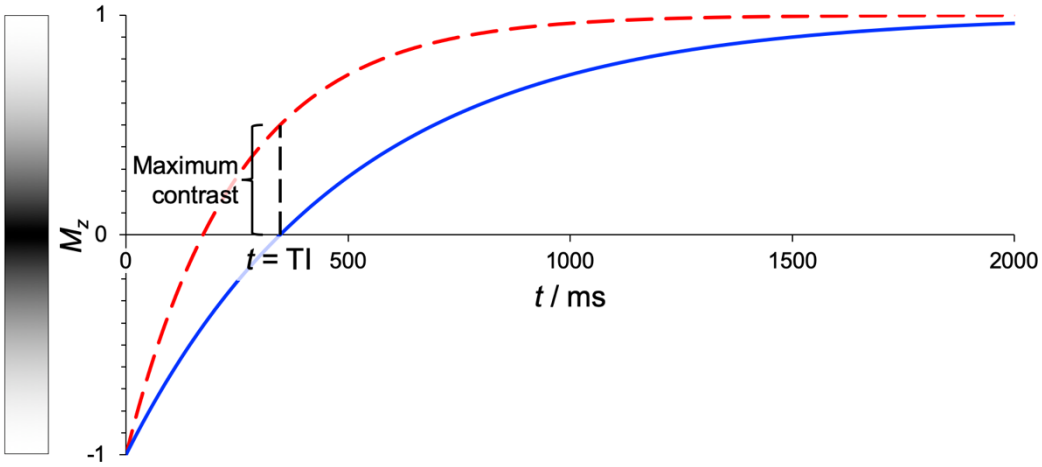

Figure 4. T_1 relaxation in LGE
This figure shows T_1 relaxation for healthy myocardium (blue solid line, T_1 500 ms) and T_1 relaxation for focally affected myocardium (dashed red line, T_1 250 ms), where T_1 is shorter due to a higher contrast agent concentration, which in turn is a consequence of an enlarged extracellular space. The inversion time (TI) has been set so that the healthy myocardium has zero magnetisation, which gives no signal, and therefor black pixels in the image, as shown in the colour scale bar on the left. At this time point TI, the contrast between the affected and healthy myocardium is at its maximum and the focally affected myocardium will appear much brighter in the image.

Herein lies both the strength and the weakness of the method. The strength is that the nulling of the signal of healthy myocardium gives a high contrast in the image that easily separates focal lesions from healthy myocardium. The drawback is that there is no sure way to tell if the healthy myocardium really is healthy. Diffuse changes affecting the whole myocardium will not be easily detected using LGE. ECV can detect these diffuse changes, which is the topic of *Study II*.

LGE has been developed further using phase-sensitive inversion recovery (PSIR), where not only the magnitude of the relaxation curve but also its phase (plus or minus) is taken into account. This makes the nulling of healthy myocardium less critical (23).

Since LGE imaging is also based on T_1 relaxation, synthetic LGE images (24) can be generated from T_1 maps, where TI can be optimized during image evaluation after image acquisition has concluded.

2 PATHOPHYSIOLOGY

2.1 EXTRACELLULAR VOLUME

The body can be divided into intra- and extracellular spaces. In the blood pool, the extracellular volume (ECV) consists of blood plasma, and in the myocardium, collagen is an important part of extracellular space (25). In the myocardium, a normal extracellular volume (ECV) fraction is 20–30 %, and a good correlation has been found between ECV measurements and the amount of fibrosis (26–28).

An increase in ECV has been found to be an important risk factor for death and hospitalisation for heart failure. A study from 2012 found that ECV, measured in myocardium excluding infarctions, was related to short-term mortality (median follow-up time 0.8 years), even when adjusting for systolic function and age, and when separately analysing patients with and without non-ischemic scars (29). Subsequent studies found that an increase in ECV was associated with mortality and/or admission to hospital for heart failure during median follow-up times of 1.3 years (30), and 1.7 years (31), respectively. A study with biopsy-verified ECV found ECV to be an independent predictor of event-free survival (median follow-up time 0.8 years), among imaging parameters but not when clinical parameters were included (27). ECV can also be measured without measuring the haematocrit and this "synthetic" ECV has also been found to be associated with mortality during a median follow-up time of 1.7 years (28).

2.2 MYOCARDITIS

Myocarditis is defined as an inflammation of the myocardium. The inflammation is often first induced by a viral infection that triggers an immune response which in turn causes damage to the tissue (32).

Myocarditis often occurs in younger adults, and has been shown to be the cause of 12 % of sudden death in younger individuals (33). Myocarditis can also cause death and heart failure in children, and sometimes heart transplantation is needed. In patients up to 18 years of age, myocarditis mostly affects teenagers (about half of the cases) and children below two years of age (about a quarter of the cases) (34).

The symptoms of myocarditis can range from chest pain to acute heart failure and it is therefore often difficult to diagnose myocarditis based on clinical information alone. A step forward was made with the introduction of the so called *Dallas criteria* for diagnosing myocarditis by endomyocardial biopsy (EMB) where an inflammatory infiltrate has to be located next to damaged myocytes in order for the diagnosis to be made (35). However, EMB is prone to sampling errors even if several biopsies are made. The problem is made worse by the fact that myocarditis often affects the inferolateral epicardial part of the left ventricle, whereas only the septum is accessible when biopsies are taken from the right ventricle, which

is most often the case. Severe procedural complications can also occur during EMB, and the total complication rate has been found to be 6 % (36).

Echocardiography can be used to evaluate left ventricular size, function, and wall thickness, but reliable myocardial tissue characterisation has not made it to clinical mainstream. Therefore, there are several reasons for developing new diagnostic tools to detect myocarditis.

CMR was first used in the 1990's for detecting myocarditis, both with and without contrast-agents, and several studies showed a high diagnostic accuracy for various combinations of CMR sequences (37). In 2009, a JACC white paper was published including expert advice for using CMR in diagnosing myocarditis (37). These recommendations were called the *Lake Louise Consensus Criteria* and stated that in cases where myocarditis is suspected clinically, CMR findings are consistent with inflammation if two of the following three criteria are fulfilled: i) signal enhancement on T_2-weighted images, either regional or global (*i e* compared to skeletal muscle); ii) T_1-weighted images showing an increased early gadolinium enhancement (EGE) ratio between myocardium and skeletal muscle; iii) late gadolinium enhancement images with one or more focal lesions with non-ischemic distribution (37).

The second criteria, EGE ratio, is claimed to detect an increased distribution volume for the gadolinium contrast agent in the vessels and in the interstitium during the so called early washout phase (37). This enhancement was thought to represent hyperaemia and capillary leakage. However, this interpretation may be questionable given that a change in enhancement only can depend on a changes in the distribution volume (38), and this does not change markedly from early to late post-contrast (39). It was later found that the removal of the EGE ratio criterion did not change the overall accuracy for detecting myocarditis, although it lowered the sensitivity (40).

Another problem raised in the white paper is that the EGE ratio, which is the ratio of early enhancement in the myocardium divided by the early enhancement in skeletal muscle, will be lower if myositis occurs at the same time (37). Furthermore, the EGE ratio has been shown to have the lowest area under the curve for identifying myocarditis compared to ECV, LGE, T_2-ratio as well as global T_1 (41).

For these reasons, we wanted to examine if there is a difference between early and late gadolinium enhancement ratios in *Study I*. To increase the measurement precision, this was performed using T_1 mapping instead of T_1-weighted images. Images from a representative patient with myocarditis are shown in Figure 5.

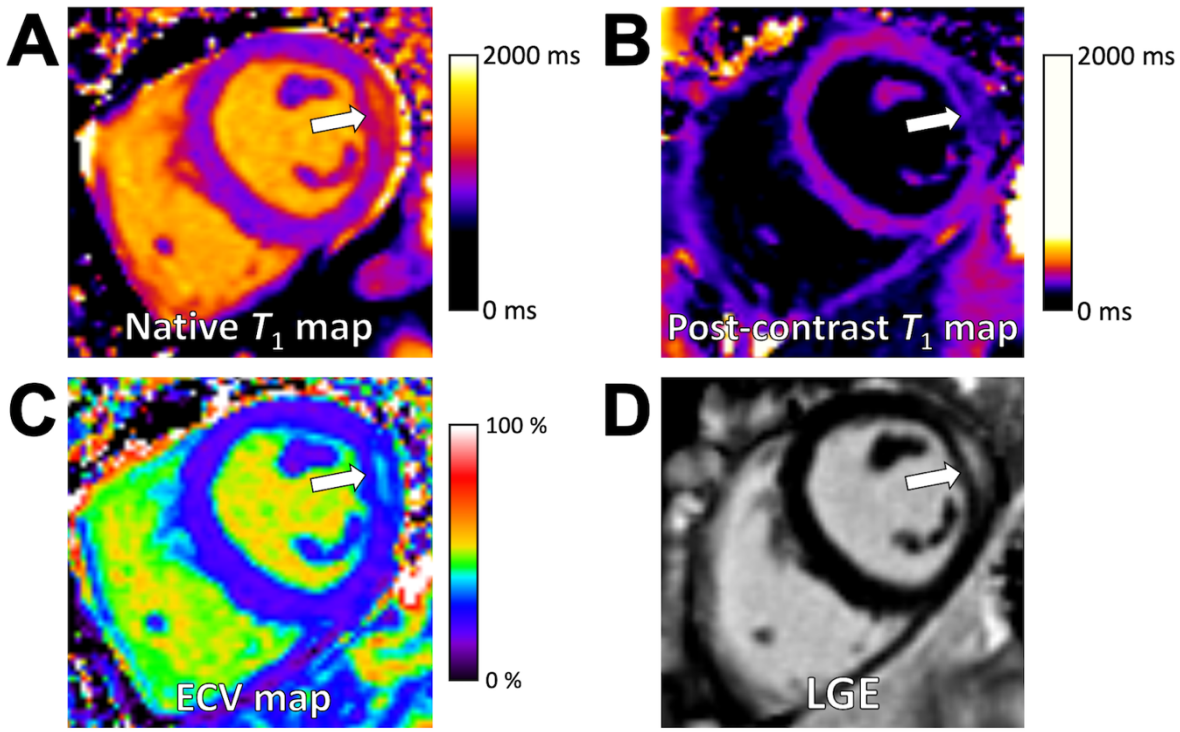

Figure 5. Images from a representative patient with myocarditis.
An example of a midventricular short-axis slice with a focal myocarditis lesion in the lateral myocardial wall (indicated by white arrows) in a representative patient with myocarditis. The images are: **A**) native (pre-contrast) T_1 map (purple is normal and orange/yellow is high myocardial native T_1), **B**) post-contrast T_1 map where the lesion is darker than other myocardium, indicating a lower T_1 which is due to a higher concentration of contrast agent, **C**) ECV map where the lesion is light blue, which indicates an ECV above 30 %, whereas the rest of the myocardium is blue/purple corresponding to the normal ECV range 20–30 %, **D**) Late gadolinium enhancement (LGE) image where the lesion has a high signal intensity and healthy myocardium is black. ECV = extracellular volume fraction; LGE = late gadolinium enhancement.

2.3 LEFT VENTRICULAR HYPERTROPHY

Cardiovascular magnetic resonance (CMR) can be used to measure mass and the volumes of the left ventricle with excellent reproducibility (43). Left ventricular hypertrophy (LVH) is typically measured as an increased left ventricular mass (LVM) or LVM indexed (LVMi) to body surface area (BSA)

LVH can be classified as *concentric hypertrophy*, where the left ventricular wall is thick but the volume is unchanged, or *eccentric hypertrophy* where the wall isn't thick but the increase in mass is caused by enlargement of the heart, where the lateral enlargement makes it eccentric in regards to the normal position of the heart (44), hence the term eccentric hypertrophy. *Concentric remodelling* is defined as increased wall thickness but normal mass

(45). There is an increased risk for adverse events for both patients with concentric remodelling (45), and for patients with LVH (46). Images illustrating these types of hypertrophy and lack thereof are shown in Figure 6.

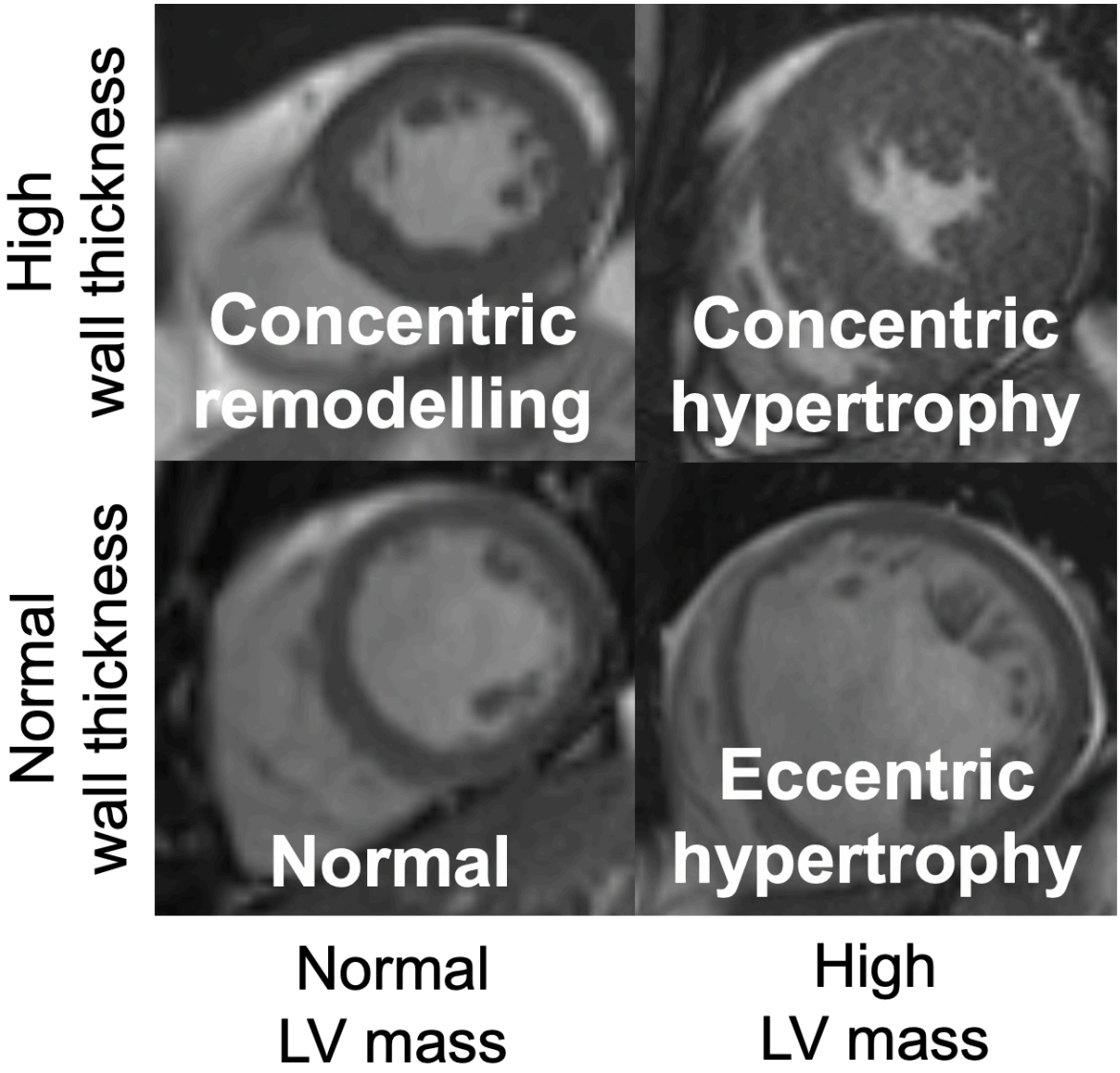

Figure 6. Examples of hypertrophy, remodelling and normal configuration. The images show (clock-wise from bottom left corner): normal configuration with normal mass and wall thickness; concentric remodelling with high wall thickness but normal mass; concentric hypertrophy where both the wall thickness and the mass are high; and eccentric hypertrophy where the mass is high but the wall thickness is normal.

Thickening walls and enlargement of the left ventricle does not need to be pathological. Athlete's heart has been defined as enlargement of the heart due to physical activity (47). There are two types of athlete's heart, one where volume loading from dynamic exercise, such as long distance running, can cause eccentric hypertrophy, and another where pressure loading from static exercise, such as weight lifting, can cause concentric hypertrophy (48).

Hypertrophic cardiomyopathy (HCM) is a genetic disorder which is characterised by an increase in LV wall thickness which affects either the whole LV or only a part of it in an asymmetric fashion. Also, patients with genetically verified HCM may not necessarily have an increased LV mass, since this may develop at a later age (49).

Among sudden death in athletes in the United States of America, HCM accounts for more than one third of the confirmed cardiovascular causes (50). It is therefore important to be able to distinguish HCM from athlete's heart in athletes (51). Patients with HCM usually have thickened walls but a ventricular septal thickness of 13–15 mm can both be caused by mild forms of HCM as well as by athlete's heart (51). An algorithm for this intermediate state has therefore been developed, and it contains both left ventricular cavity size, left atrial enlargement, prominent ECG changes, as well as other findings (51).

On echocardiography, classification of hypertrophy is based on the linear measure relative wall thickness (RWT), where the thickness of the left ventricular wall is measured in end diastole and divided by the end-diastolic diameter of the left ventricle. RWT can be calculated from the interventricular septal wall thickness at end diastole (IVSd) and/or the posterior wall thickness at end diastole (PWd), divided by the left ventricular end-diastolic dimension (LVEDD), as 2 × IVSd/LVEDD, or 2 × PWd/LVEDD, or (IVSD+PWd)/LVEDD. In patients with high LV mass, RWT is high in concentric hypertrophy and normal in eccentric hypertrophy, whereas patients with high RWT but normal mass are classified as having *concentric remodelling* (52). Sub-classification of LV remodelling has been proposed using a combination of volume, mass and relative wall thickness into as many as six categories (53).

Another measure that can be used to characterise the left ventricle is concentricity$^{0.67}$, which is calculated as LVM divided by LVEDV$^{0.67}$ (54). The rationale for this measure is that the area (wall) of a sphere is calculated using the square of the radius whereas the volume of the sphere is calculated using the cube of the radius, taking LVEDV$^{0.67}$ would thus give a ratio independent of the radius. Others have proposed using a combination of concentricity$^{0.67}$, LV volume relative to BSA, and LVM relative to either height$^{2.7}$ (54) or BSA (55).

However, both relative wall thickness and mass-to-volume ratio have inherent methodological shortcomings where the former only measures the wall thickness in one location and none of them takes body size into account, and this may limit their diagnostic discriminatory ability. The use of three measures, such as concentricity$^{0.67}$, mass and volume, also makes classification somewhat cumbersome and this could potentially be simplified.

In *Study III*, we hypothesized 1) that it should be possible to estimate the global left ventricular end-diastolic mean wall thickness (GT) from CMR measures of LV mass and LV end-diastolic volume, 2) that the estimated GT could be used together with LV mass index to distinguish between different forms of hypertrophy, and 3) that survival could be used as an arbiter to determine which measures of hypertrophy were most appropriate for clinical use.

3 AIMS

The specific aims of the four studies were:

Study I: To use T_1 mapping to determine whether there are any benefits of performing contrast enhanced imaging early or late post-contrast, with regards to detecting patients with acute myocarditis.

Study II: To determine the prevalence of both diffusely increased ECV in remote myocardium and of focal LGE findings in a clinical population, and to explore how these findings relate to left ventricular size, mass, and systolic function.

Study III: To derive and validate a new measure for global wall thickness that can be calculated from known parameters; to evaluate the prognostic performance of this new measure of wall thickness and other related measures; to use the most prognostic measure together with LV mass for classifying different types of hypertrophy; and finally to determine the outcomes for the same types of hypertrophy.

Study IV: To develop and apply a clinical method for measuring the myocardial intracellular lifetime of water (τ) in patients with different types of left ventricular hypertrophy in order to evaluate the clinical feasibility of measuring τ.

4 MATERIALS AND METHODS

4.1 STUDY POPULATIONS

All four studies contain patients from the database KAMRAT which was compiled for *Study II*. The patients were included in the database from September 2013 up until November 2015 when 1000 patients had been included.

These patients underwent CMR at 1.5 (Siemens Aera, Siemens Healthineers, Erlangen, Germany) at Karolinska University Hospital in Solna, Sweden. They were all referred for known or suspected disease involving the heart or the great vessels, and some were scanned as part of inclusion in other studies.

4.1.1 Study I

Patients were retrospectively identified from the KAMRAT database described above. The patients with myocarditis (n = 19) were diagnosed as having acute myocarditis by CMR. Acute presentation was defined as having a time between the start of the symptoms and the exam had being no more than four weeks. Since only one short-axis slice was imaged early post-contrast, both healthy and affected myocardium had to be identified in this slice.

The controls (n = 19) were also identified from the KAMRAT database but had normal findings with normal ventricular volumes, normal systolic function, and no focal myocardial lesions or myocardial oedema.

4.1.2 Study II

This study was mainly based on the whole KAMRAT database but only included patients with clinical reports containing left ventricular volumes, mass and systolic function as well as measures of ECV and native T_1 measured remotely from any focal lesions, and analysed LGE images. Since the main objective of *Study II* was to evaluate remote ECV, exclusion criteria were patients with amyloidosis since they are known to have areas of extremely high ECV, and hypertrophic cardiomyopathy, which is a unique genetic disorder. Only the first complete exam was included for patients with multiple exams. The final number of patients in the study was 609.

Healthy volunteers (n = 38) were also included in order to establish the normal range for ECV. These subjects were originally included for another study (56), and these volunteers had no medical history of cardiovascular disease, kidney disease, or asthma, had no previous or current use of cardiovascular drugs, and none were current smokers.

4.1.3 Study III

This was a relatively large study with regards to number of patients, with a total of 2543 subjects being included to address the various aims of the study.

4.1.3.1 Derivation and validation cohort

The *derivation and validation cohort* was identified to derive and validate the new measure global wall thickness (GT). The cohort was made up of 537 test subjects and included healthy volunteers, endurance athletes, heart failure patients, patients with a recent myocardial infarction, and patients with unexplained chest pain, also known as cardiac syndrome X.

The healthy volunteers were examined between 2001 and 2009, and included both young and old subjects who had no history of hypertension, or cardiovascular or systemic disease. The endurance athletes were competing in triathlon, football/soccer, handball, or swimming on an elite national level. They were scanned between 2005 and 2008. The patients with heart failure were candidates for implantation of a cardiac resynchronization therapy (CRT) pacemaker and underwent CMR between 2010 and 2014. The group of patients with myocardial infarction patients had an acute myocardial infarction and were included in several multicentre trials between 2011 and 2015. The patients with cardiac syndrome X underwent CMR between 2011 and 2016.

All groups consisted of both males and females. This diverse group of patients were divided into a derivation cohort and a validation cohort, with an as equal as possible distribution of males and females from each diagnosis group in each cohort.

4.1.3.2 Survival cohort

The patients of the survival cohort (n = 1575) were consecutively included at the University of Pittsburgh Medical Center between 2010 and 2016. These patients have been studied previously with regards to prognostic outcome (57) but they have not been examined with regards to identifying and comparing various measures of left ventricular hypertrophy. Patients with amyloidosis were excluded since it is such a particular phenotype where an increased wall thickness can be caused by myocardial infiltration rather than cellular hypertrophy.

4.1.3.3 Test-retest cohort

To evaluate the repeatability of our new measure of wall thickness, a test-retest cohort (n = 101) was identified. This cohort included both healthy volunteers and patients with various pathologies. The subjects underwent CMR at various locations in the United Kingdom during 2010 to 2019.

4.1.3.4 Mixed cohort

In order to establish a range of normal values for the new wall thickness measures, the healthy volunteers from the *derivation and validation cohort* were supplemented with an additional 23 patients scanned in 2016, some of which were also included in *Study II*. This gave a total of 100 volunteers, but one of the female volunteers was found to have a highly abnormal global wall thickness index (GTi) that was four standard deviations above the mean

GTi for the other female volunteers. This case was removed since the test subject clearly was an outlier, and the final number of healthy volunteers was 99.

To determine the performance of the new measures in additional patient groups, patients with a prominent left ventricular hypertrophy (n = 163) were included from the KAMRAT database and they all had a left ventricular mass index (LVMi) more than three standard deviations higher than the sex-specific mean, determined from the healthy volunteers above. Patients with Fabry disease (n = 144) were also included, they all had genetically confirmed disease and underwent CMR at The Heart Hospital (London, United Kingdom) between 2011 and 2016.

4.1.4 Study IV

The patients for *Study IV* were retrospectively identified from the KAMRAT database, described previously. Four groups of patients with different combinations of LVMi and GTi, evaluated in terms of Z scores from the mean of healthy volunteers per sex, these were the same healthy volunteers used in *Study III*. The patients with *concentric hypertrophy* were identified by having the highest combination of LVMi and GTi in terms of the Z score for LVMi times the Z score of GTi divided by the sum of their Z scores; patients with *eccentric hypertrophy* had the highest Z scores for LVMi while still having a normal GTi; the patients with *concentric remodelling* on the other had the highest GTi but still having a normal LVMi; and the patients with *normal configuration* were as close to zero in terms of Z scores for both GTi and LVMi.

Patients could only be included if they had overlapping midventricular short-axis T_1 maps acquired before and at three time points post-contrast. Patients were excluded if: 1) there were artefacts, lesions or scars involving more than two segments (up to two segments could be excluded in the analysis), 2) the administered dose of contrast agent was lower than 0.15 mmol/kg body weight, or 3) if the patient was diagnosed with Fabry disease or amyloidosis which both affect native T_1.

4.2 IMAGING AND ANALYSIS

4.2.1 Study I

It is important to clarify comparative measures comparing studies using different techniques such as signal intensities from T_1-weighed images as opposed to magnetisation characteristics like T_1. These are summarised in Table 1. The T_1-weighted signal intensity (SI) used in the older studies corresponds to R_1 ($1/T_1$), and the signal enhancement (SE) which is calculated as $(SI_{post\text{-}contrast} - SI_{pre\text{-}contrast})/SI_{post\text{-}contrast}$ corresponds to $\Delta R_1/R_{1\ pre\text{-}contrast}$. These enhancement measures correspond to Early gadolinium enhancement (EGE) when the post-contrast images are acquired early. Moreover, global relative enhancement ($GRE = SE_{myocardium} / SE_{skeletal\ muscle}$) can be calculated from T_1 maps as $(\Delta R_{1\ myocardium} / R_{1\ myocardium,\ pre\text{-}contrast})/(\Delta R_{1\ skeletal\ muscle} / R_{1\ skeletal\ muscle,\ pre\text{-}contrast})$.

Table 1. Comparison of quantitative measures by T_1-weighted imaging and T_1 mapping. The table shows the T_1-weighted measures and their corresponding T_1 mapping measures, and how to calculate these. a.u. = arbitrary units; ECV = extracellular volume fraction; EGE = early gadolinium enhancement; GRE = global relative enhancement; hct = haematocrit; SE = signal enhancement; SI = signal intensity. §These measures are not typically reported using T_1-weighted imaging but are included for purposes of comparison and completeness.

T_1-weighted imaging measure		**Corresponding T_1 mapping measure**	
Signal intensity [a.u.]	= SI	Relaxation rate [sec^{-1}]	= $R_1 = 1/T_1$
Difference in SI [a.u.], which is not linearly proportional to contrast agent concentration §	= ($SI_{post\text{-}contrast}$ - $SI_{pre\text{-}contrast}$)	Difference in R_1 between pre- and post-contrast [sec^{-1}], which is linearly proportional to contrast agent concentration	= ΔR_1 = ($R_{1post\text{-}contrast}$ - $R_{1pre\text{-}contrast}$)
Signal enhancement, SE [%] = early gadolinium enhancement, EGE, when acquired early post-contrast	= ($SI_{post\text{-}contrast}$ - $SI_{pre\text{-}contrast}$)/ $SI_{pre\text{-}contrast}$	EGE equivalent, ΔR_1 divided by R_1 pre-contrast [%]	= $\Delta R_1/R_{1pre\text{-}contrast}$
Global relative enhancement, GRE [unitless ratio]	= $SE_{myocardium}/SE_{skeletal\ muscle}$	GRE equivalent [unitless ratio]	= ($\Delta R_{1\ myocardium}/R_{1\ myocardium,\ pre\text{-}contrast}$) / ($\Delta R_{1\ skeletal\ muscle}/R_{1\ skeletal\ muscle,\ pre\text{-}contrast}$)
Relative enhancement, compared to blood [unitless ratio] §	= $SE_{myocardium}/SE_{blood}$	ECV [%]	= $\Delta R_{1\ myocardium}/\Delta R_{1\ blood}$ • (1 - hct)

In the T_1 maps of a midventricular short-axis slice, six regions of interest (ROIs) were placed in the midmural half of the left ventricular myocardial wall corresponding to segments 7 through 12 in the 17-segment model of the left ventricle proposed by the American Heart Association (AHA) (58), see Figure 7. In order to be included, the patients had to have both affected and unaffected segments in the imaged short-axis slice. Segments were said to be affected either by having a native T_1 above 1050 ms or if the mean native T_1 of the affected segments was at least 50 ms higher than the mean native T_1 of the unaffected segments in the same slice.

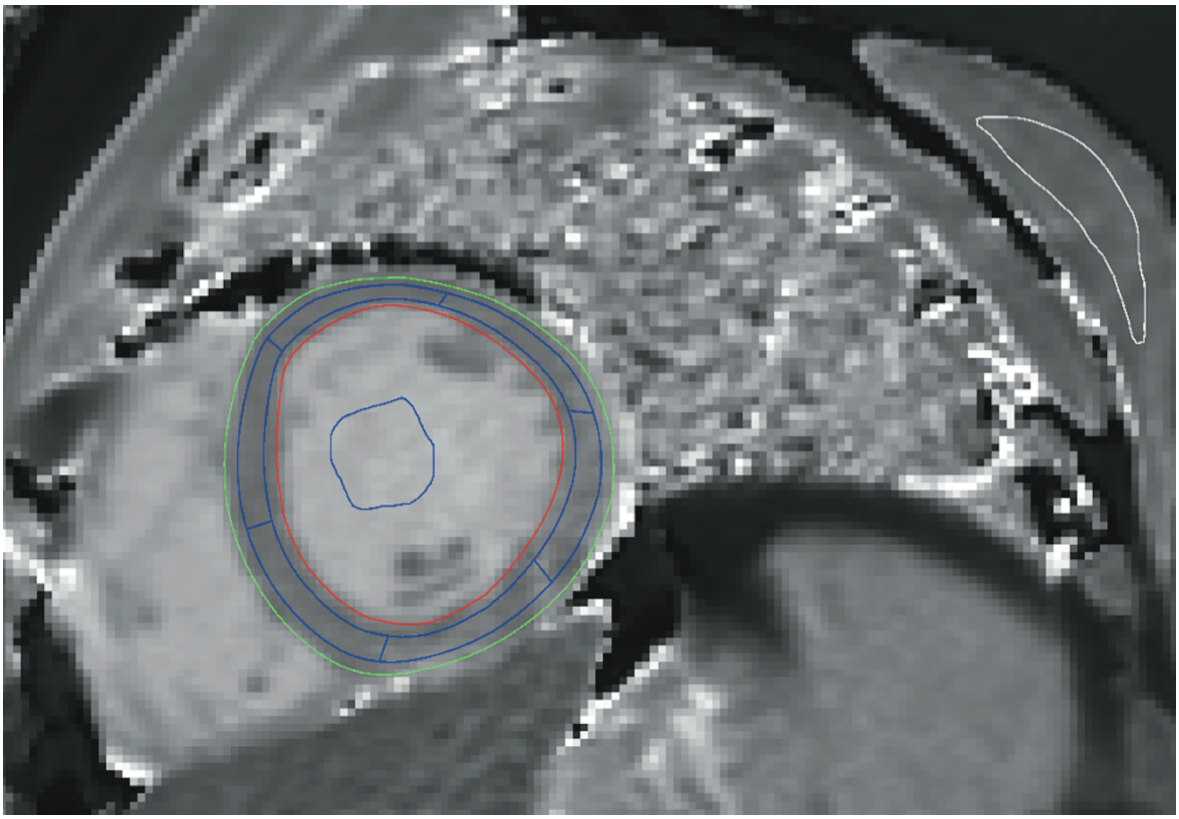

Figure 7. A representative example of a midventricular short-axis native T_1 map.
The left ventricular (LV) endocardium is outlined in red and the epicardium in green, with six blue regions of interest (ROIs) placed in the midmural 50 % of the myocardium. A blue ROI is placed in the LV blood pool and a white ROI is placed in the dorsal skeletal muscle. LV = left ventricular; ROI(s) = Region(s) of interest.

ROIs were also placed in the left ventricular blood pool and in dorsal skeletal muscle, see Figure 7. The ROIs were drawn on the native T_1 maps and then copied to the post-contrast T_1 maps with small adjustments in position being made when necessary.

4.2.2 Study II

The patients in *Study II* were analysed as a part of clinical routine using *syngo.via* (Siemens Healthineers, Erlangen, Germany) where the left ventricular endocardial and epicardial borders were outlined, with papillary muscles and trabeculations being included in the blood pool and not being included in the myocardium. The left ventricular volumes and mass were indexed to body surface area (BSA) calculated according to Mosteller (59). LGE images were examined for focal lesions and these were identified visually and reported when found. ECV and native T_1 were measured in the corresponding short-axis maps, most often in the midmural part of the inferior section of the septum but always remotely from any scars or other focal abnormalities.

The normal ranges for ECV were determined from healthy volunteers (n = 38, 50 % female) were ECV was measured in midventricular short-axis images in the midmural third of the septum. The upper limit was found to be 31 % for females and 30 % for males and these limits were used in the analysis of the patients.

4.2.3 Study III

All 2543 subjects of this study underwent CMR including steady state free precession (SSFP) cine imaging of the left ventricle. In the short-axis image stacks, the endocardial and epicardial borders were delineated in end systole and end diastole for measuring the left ventricular volumes and mass, where the mass excluded the papillary muscles and trabeculations were included in the blood pool. Volumes, mass, and other measures were index to body surface area (BSA) calculated using the Mosteller method (59).

4.2.3.1 Derivation of validation of global wall thickness (GT)

A new plug-in for the software Segment was developed in-house for purposes of measuring global wall thickness (GT) in order to validate the method for estimating GT. The plugin was used to measure GT from the test subjects' cine images that had been analysed previously with the endocardial and epicardial borders stored. For every short-axis slice containing both blood pool and myocardium, the distance between the endocardial and epicardial borders was automatically measured at 24 equally spaced point along the circumference of each slice. Areas with a wall thickness of less than 2 mm were excluded since this constituted the outflow tract. The mean wall thickness of each slice was weighted to the mid-mural circumference of each slice in order to obtain the global wall thickness, representative of the whole left ventricle. A schematic illustration of the method for measuring GT is shown in the supplementary material for *Study III,* Figure S1.

Geometrically, the wall thickness can only depend on the left ventricular mass and volume, and it should therefore be possible to calculate the wall thickness from these two measures. Mass and volume are always analysed in the clinical setting and a simple equation would obviate the need for a special plug-in or other software. The following equation was therefore proposed

$$GT = A + B \bullet LVM^X \bullet LVEDV^Y \quad \text{(Equation 7)}$$

where GT is mean global wall thickness, LVM is left ventricular mass, and LVEDV is left ventricular end-diastolic volume, and A, B, X, and Y are unknown constants that need to be determined. The derivation and validation cohort was split into a derivation cohort and a validation cohort with an as equal representation of diagnosis groups and sexes in the two cohorts. The mathematical software Matlab (R2016, Mathworks, Natick, Massachusetts, USA) was used to identify best fits for A, B, X and Y from Equation 7 by minimizing the sum of least squares to the measured wall thicknesses of the derivation cohort.

4.2.3.2 Prognostic analysis

For the prognostic analysis of the survival cohort, the time from the CMR exam to a composite end-point of death from all causes or hospitalisation for heart failure (HHF), which has been described previously (31).

4.2.4 Study IV

T_1 mapping was performed using MOLLI 5(3)3 before contrast, as well as early and late post-contrast, whereas a 4(1)3(1)2 MOLLI was used for the intermediate post-contrast imaging due to this being the clinical standard at the time. The patients received an intravenous bolus dose of a gadolinium-based contrast agent (gadoteric acid (Dotarem, Gothia Medical, Billdal, Sweden) 0.2 mmol/kg body weight) and the images were acquired early (median [interquartile range] 3.0 [2.5–4.0] minutes), intermediate (11 [8–13] minutes) and late (20 [18–24] minutes) post-contrast.

The analysis of the images in *Study IV* was similar to that of *Study I* with six regions of interest (ROIs) placed in the midmural half of the left ventricular myocardial wall. Similarly, an ROI was also placed in left ventricular blood pool in both T_1 and T_1^* maps. The ROIs were drawn on the native T_1 maps and copied to the post-contrast maps, again with small adjustments in position being made when necessary. If one or at most two segments were affected by artefacts or a focal lesion, these segments were excluded.

A model for slow exchange transcytolemmal water exchange (60) was implemented in Matlab (R2018B, Mathworks, Natick, Massachusetts, USA). The Matlab code used to perform the calculations is included in the Appendix of the manuscript for this study. The model uses R_1 (=1/T_1) of the myocardium and of the blood, both before and at three time points post-contrast. A curve is fitted to these four points and the intracellular lifetime of water (τ) and ECV are obtained from the curve fitting. See Figure 17 for examples of R_1 curves.

τ was calculated for all included segments of the myocardium and the resulting τ results were then averaged to yield the total average τ for the patient. ECV was calculated both using the model for slow exchange where all time points are used, and the commonly used fast exchange model where only the pre- and late post-contrast T_1 maps are used.

5 RESULTS

5.1 STUDY I

5.1.1 Affected versus remote segments

In the patients with acute myocarditis (n = 19), native T_1 was, by design, higher in affected compared to remote segments (median [inter-quartile range], 1090 [1071–1128] versus 1003 [993–1020] ms, $p < 0.001$). The difference in native T_1 between the affected and the remote segments was 83 [59–129] ms. The EGE equivalent measure was higher in affected versus remote segments both early and late, but the difference was higher late than early post-contrast (34±5 % versus 30±4 %, $p = 0.02$).

ECV was also higher in affected than in remote segments both early (27±1 % versus 23±1 %, $p < 0.001$) and late post-contrast (31±1 % versus 26±1 %, $p < 0.001$). The difference in ECV between affected and remote segments however was higher late than early post-contrast (5.3±0.7 % versus 4.0±0.6 %, $p = 0.002$), see Figure 8.

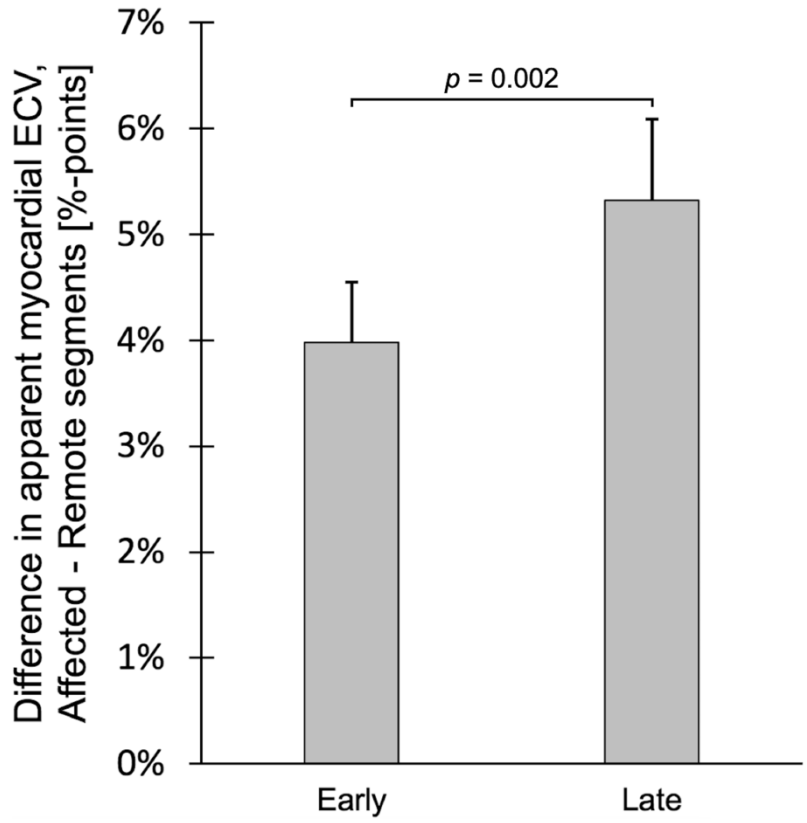

Figure 8. Difference in apparent myocardial ECV between affected and remote segments.
The difference in apparent myocardial ECV between affected and remote segments was higher late compared to early post-contrast in patients with myocarditis. The whiskers show the standard error of the mean. ECV = extracellular volume fraction.

5.1.2 Myocarditis versus controls

When comparing myocarditis patients to controls (n = 19), the GRE equivalent of the whole short-axis slice was higher in the myocarditis patients compared to controls both early post-contrast (5.1 [4.5–6.5] versus 3.4 [2.5–4.5], $p < 0.001$) as well as late post-contrast (3.0 [2.6–3.7] versus 2.0 [1.7–2.4], $p < 0.001$) as shown in Figure 9. Native T_1 and ECV of skeletal muscle were both lower in the myocarditis patients compared to controls: 876 [843–915] ms versus 916 [896–939] ms, $p = 0.02$ for native T_1 of skeletal muscle and both early post-contrast ECV (5.1 [4.3–6.2] % versus 7.6 [5.7–9.0] %, $p = 0.03$) and late post-contrast ECV (10.2 [9.7–12.8] % versus 13.0 [11.4–15.7] %, $p = 0.004$), see Figure 9.

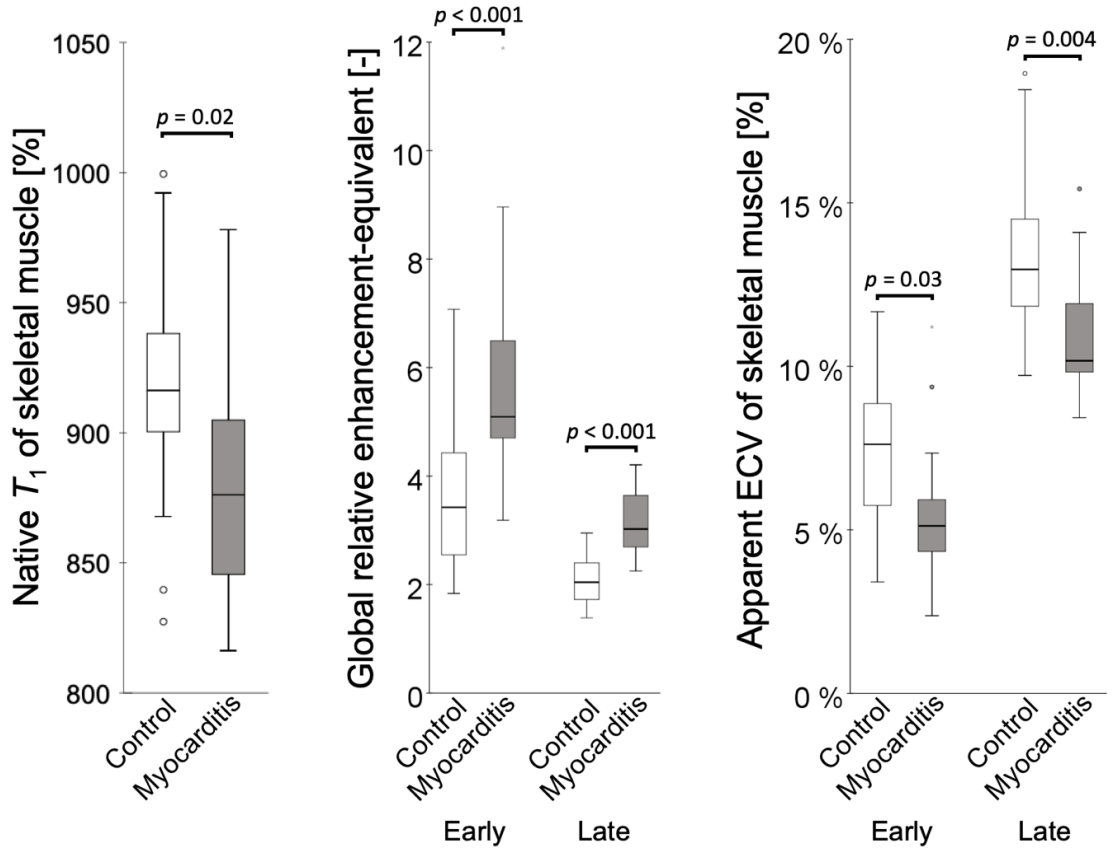

Figure 9. The global relative enhancement equivalent and comparisons between dorsal skeletal muscle in myocarditis patients and in controls .
The global relative enhancement (GRE) equivalent for the myocardium of the entire short-axis slice (center), including both remote and focally affected myocardium, was higher in myocarditis patients (grey boxes) than in controls (white boxes) both early and late post-contrast. The GRE equivalent in T_1 mapping is calculated as: $(\Delta R_{1\text{myocardium}}/R_{1\text{myocardium, pre-contrast}}) / (\Delta R_{1\text{skeletal muscle}}/R_{1\text{ skeletal muscle, pre-contrast}})$. Both the native T_1 of skeletal muscle (left) and the apparent ECV of skeletal muscle early and late post-contrast (right) was lower in myocarditis patients compared to controls. ECV = extracellular volume. The boxes show the interquartile range, the bar in the box shows the median and the whiskers show the range, except for outliers which are shown as circles or stars.

5.1.3 Remote myocardium versus controls

When comparing the remote myocardium of the myocarditis patients to the controls, the GRE equivalent was higher in the patients' remote myocardium both early (5.0 [4.3–5.3] versus 3.4 [2.5–4.5], $p = 0.002$) as well as late post- contrast (2.8 [2.4–3.1] versus 2.0 [1.7–2.4], $p < 0.001$). Native T_1 was also higher in the myocarditis patients' remote myocardium than in controls (1003 [993–1020] versus 996 [966–1007] ms, $p = 0.03$), but only to a small degree. Conversely, ECV did not differ between the remote myocardium of the myocarditis patients compared to the controls either early (22.7±0.9 % versus 21.7±0.4 %, $p = 0.37$) or late post-contrast (25.8±0.7 % versus 25.2±0.5 %, $p = 0.52$), see Figure 10.

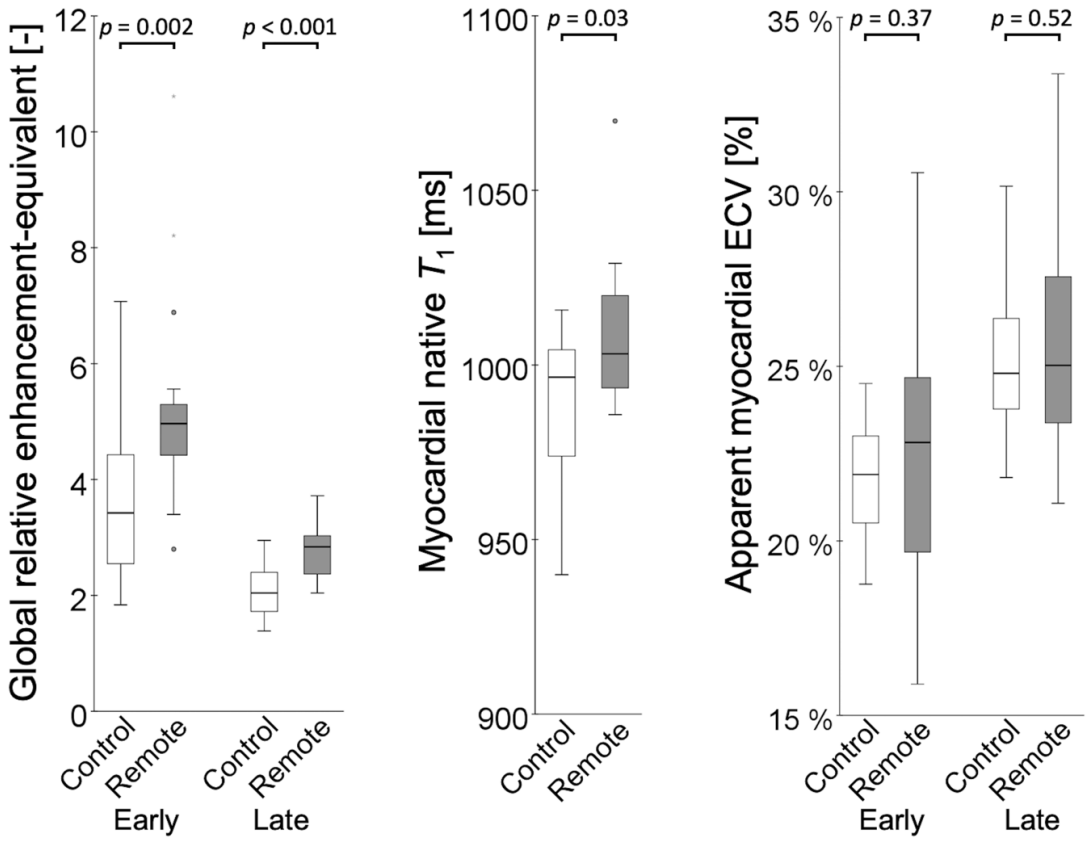

Figure 10. Comparisons between remote myocardium in myocarditis patients and controls.

The remote myocardium of the myocarditis patients (grey boxes) and the myocardium of the controls (white boxes) differed in GRE equivalent (left), and in native T_1 (centre), but not in apparent myocardial ECV (right). ECV = extracellular volume. The box plot is used since the relative contrast concentration early post-contrast as well as myocardial native T_1 in myocarditis patients did not follow a normal distribution; the Mann–Whitney *U* test was used for these two measures, and the unpaired *t*-test was used for the remaining measures. The boxes show the interquartile range, the bar in the box shows the median and the whiskers show the range, except for outliers which are shown as circles or stars.

5.2 STUDY II

Increased remote ECV was found in 50 out of 609 patients (8 %), 30 of these 50 the patients with increased ECV did not have focal LGE findings, see Figure 11.

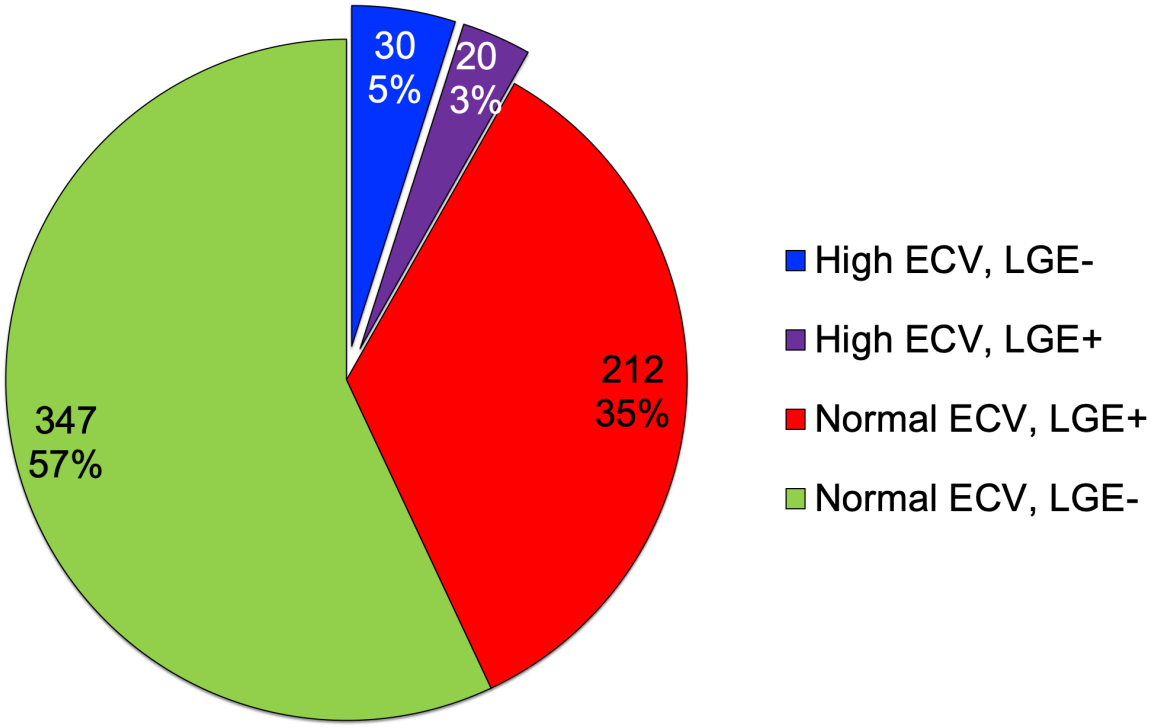

Figure 11. ECV and LGE findings.
The limit for high ECV was set to remote ECV above 31 % for females and 30 % for males. LGE+ indicates focal LGE findings and LGE- absence thereof.

An increase in remote ECV was more common in patients with a pronounced LV dilatation ($p < 0.001$), in patients with a pronounced increase in LV mass index (LVMi) ($p = 0.04$) and in females (13.0 % versus 5.3 % in males, $p < 0.001$) whereas the prevalence of increased ECV did not differ in patients with or without a pronounced decrease in left ventricular ejection fraction (LVEF), see Figure 12

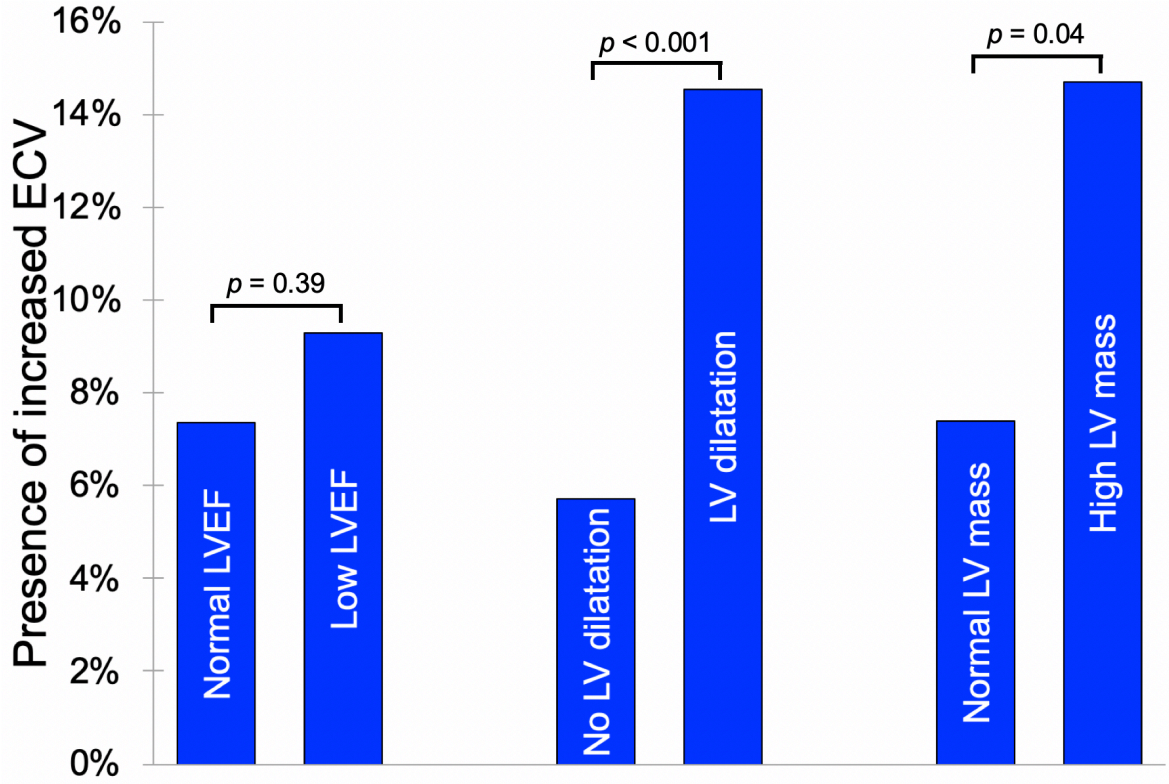

Figure 12. Prevalence of diffusely increased ECV

The figure shows the prevalence of diffusely increased ECV in patients with and without pronounced abnormalities in LVEF, LV dilatation, and LV mass respectively. LV=left ventricular; LVEF=left ventricular ejection fraction.

Focal LGE on the other hand was more common patients with a pronounced decrease in LVEF ($p < 0.001$) but the prevalence in LGE did not differ for patients with or without pronounced increases in LVMi ($p = 0.06$) or pronounced dilatation ($p = 0.52$), see Figure 13

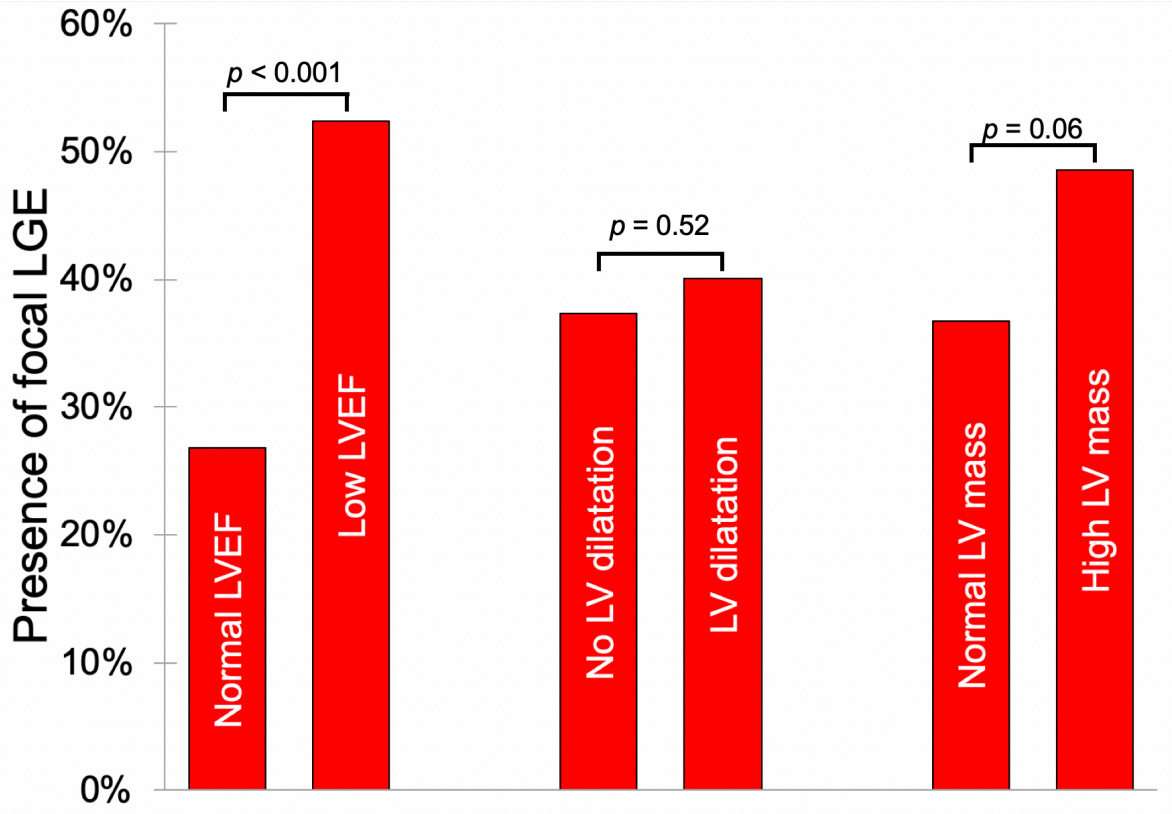

Figure 13. Prevalence of focal LGE
The figure shows the prevalence of focal LGE findings in patients with and without pronounced abnormalities in LVEF, LV dilatation, and LV mass respectively. LGE=late gadolinium enhancement; LV=left ventricular; LVEF=left ventricular ejection fraction.

Similar results were obtained using logistic regression where a pronounced decrease in LVEF was associated with LGE ($p < 0.001$) but not with a high ECV ($p = 0.41$). On the other hand, pronounced LV dilation was associated with a high ECV ($p = 0.001$) but not with the presence of LGE ($p = 0.054$).

The normal limits used for ECV were indirectly confirmed by examining patients with normal finding. The females with normal findings had a remote ECV of 27.0±2.0 % which corresponds to an upper limit of 31 % and the males had a remote ECV of 24.8±1.6 %, corresponding to an upper limit of 28 %.

When used together, ECV mapping and native T_1 mapping can be used to diagnose a wide range of conditions, see Figure 14.

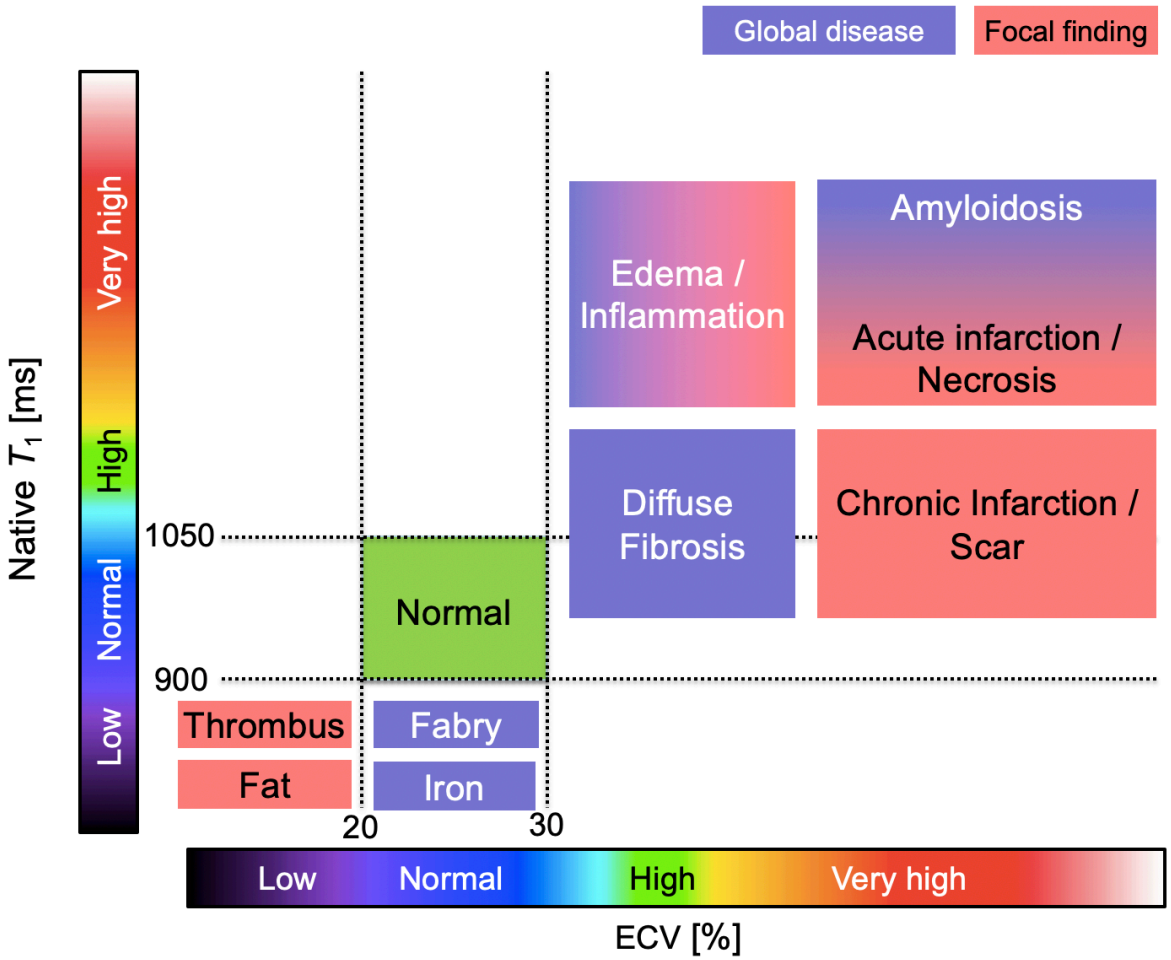

Figure 14. Diagnostic diagram for native T_1 and ECV.
This diagram shows some examples of both global (blue) and focal (red) abnormalities that can be diagnosed using native T_1 and/or ECV mapping. Please note that the limits for native T_1 reflect conditions at 1.5 T and using our setup, that the upper limit for ECV for males is shown and that the upper limit for females was 1 %-point higher in our study.
Adapted from Martin Ugander (SCMR 2014).

5.3 STUDY III

5.3.1 Calculating global wall thickness (GT)

The fitting of the parameters of $GT = A + B \bullet LVM^X \bullet LVEDV^Y$ (Equation 7) for calculating GT, to the measured wall thickness results of the derivation cohort resulted in the following equation:

$$GT = 0.05 + 1.60 \bullet LVM^{0.84} \bullet LVEDV^{-0.49} \quad \text{(Equation 8)}$$

where GT is the global wall thickness measured in mm, LVM is mass of the left ventricular myocardium measured in grams, and LVEDV is left ventricular end-diastolic volume measured in millilitres. This equation (Equation 8) was then used for all other patients with no extra plug-in or application needed. The correlation between measured wall thickness and

calculated GT was found to be very high for both the derivation and the validation cohort, $R^2 = 0.95$, $p < 0.001$ for both. There was no bias for the derivation cohort (0.00±0.24 mm) and very low bias for the validation cohort (0.01±0.23 mm), with low standard deviation for both cohorts. The standard deviation of the bias for the validation cohort implies a 95 % confidence interval if only 0.45 mm.

5.3.2 Normal ranges for GT

In the 99 healthy volunteers GT was found to be 5.9±0.6 mm and 7.2±0.7 mm for females and males, respectively, corresponding to normal ranges of 4.8–7.1 mm and 5.8–8.5 mm for females and males, respectively.

In the healthy volunteers GT indexed (GTi) to body surface area (BSA) was found to be 3.4±0.4 mm/m^2 and 3.6±0.4 mm/m^2 for females and males, respectively, which corresponds to normal ranges of 2.7–4.1 mm/m^2 and 2.9–4.3 mm/m^2 for females and males, respectively.

For both sexes, both athletes and all patient groups had higher GT than the healthy volunteers ($p < 0.02$ for all groups separately for both sexes) with similar results for with GTi except for the CRT candidates which did not differ ($p < 0.02$ for both sexes for all groups except for CRT candidates).

5.3.3 Test–retest

The test-retest cohort ($n = 101$) was examined for test-retest variability for various measures and the variability was lowest for GT at 4.2 %. The highest variability was found for EDV and mass-to-volume ratio (6.1 % and 6.2 %, respectively, $p < 0.001$ for both versus GT).

5.3.4 Prognostic analysis

When analysing the whole *survival cohort* ($n = 1575$, 42 % female, follow-up time 5.4 [3.9–6.4] years) by univariable Cox regression, it showed that the parameter with the highest prognostic value for hospitalisation for heart failure (HHF) or death, apart from age at CMR and presence of hypertension, was LVMi (χ^2 66.7, $p < 0.001$) followed by GTi (χ^2 37.3, $p < 0.001$) and GT (χ^2 33.1, $p < 0.001$). In multivariable analysis including both LVMi and GTi, LVMi was associated with outcomes ($p < 0.001$) and GTi was not ($p = 0.60$). For more details, see Table 1 of *Study IV*.

When analysing only the patients with normal findings for LVEDVi, LVMi, LVEF and no LGE ($n = 326$, 45 % female, follow-up time 5.8 [5.0–6.7] years) in the same way as above, the most prognostic parameters for the composite end-point HHF or death were GT (χ^2 26.8, $p < 0.001$) and concentricity$^{0.67}$ (χ^2 26.6, $p < 0.001$), and these were more prognostic than both hypertension (χ^2 23.5, $p < 0.001$) and age at CMR (χ^2 14.5, $p < 0.001$). When multivariable analysis was performed including LVMi and GT, LVMi was not associated with outcomes ($p = 0.70$) but GT was ($p = 0.01$), see Table 2 of *Study IV*.

5.3.5 Classification by GTi and LVMi

Patients of the *mixed cohorts* (who were not part of the prognostic cohort) were classified using GTi and LVMi, these numbers being indexed according to the mean and measured in standard deviations from the mean of the healthy volunteers per sex, see Figure 15. The patients with left ventricular hypertrophy were mostly classified as having concentric hypertrophy and patients with heart failure who were candidates for CRT implantation were mainly classified as having eccentric hypertrophy. Most endurance athletes were classified as normal but a fair amount as having eccentric hypertrophy. Although the median patient with Fabry disease was classified as having concentric hypertrophy, a large variability was seen both in terms of GTi and LVMi corresponding to the large variability of the disease. The healthy volunteers, the patients with normal findings, and the patients with acute myocardial infarction were all mainly classified as being normal.

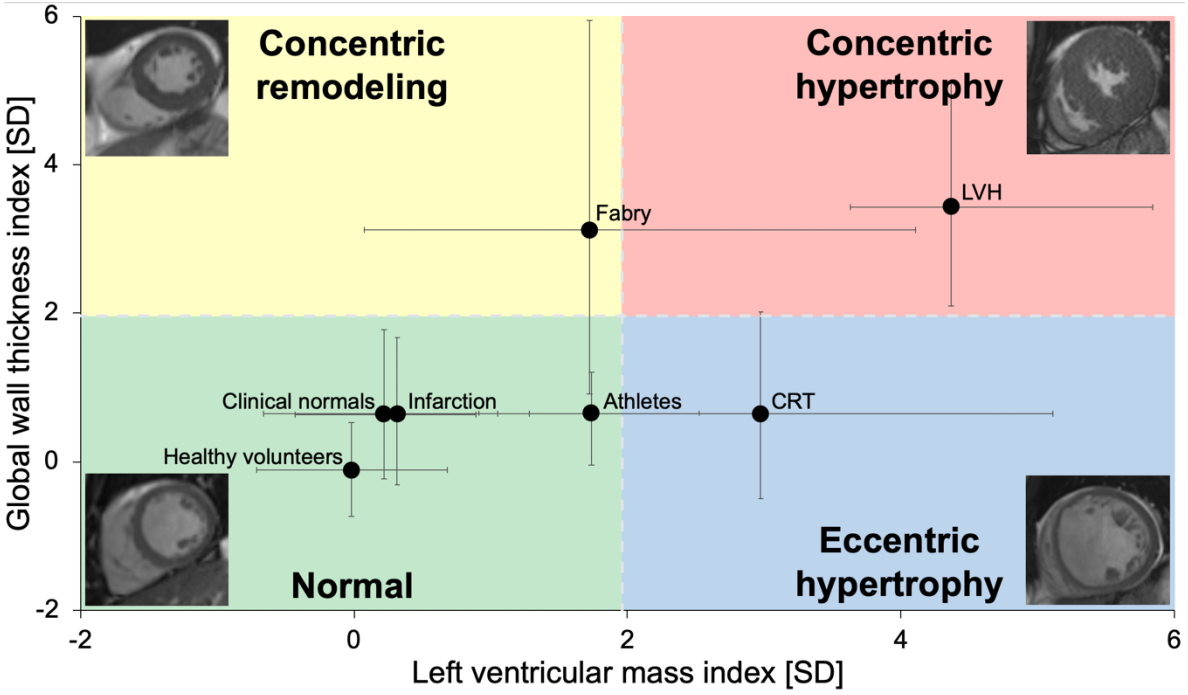

Figure 15. Characterisation of left ventricular hypertrophy using wall thickness and mass.

The patient groups of the *mixed cohort* were classified according to their global wall thickness index (GTi) plotted against their left ventricular mass index (LVMi). The solid circles show the median and the whiskers show the interquartile range. Both GTi and LVMi were indexed to standard deviations (SD) from mean of the healthy volunteers per sex. The coloured fields show the proposed classification of hypertrophy based on LVMi and the new measure GTi. The grey dashed lines between the coloured fields indicate the upper limit of normal (+1.96 SD) for both measures. The mixed cohort consist of healthy volunteers, endurance athletes, cardiac resynchronization therapy (CRT) candidates, patients with recent acute ST-elevation myocardial infarction (Infarction), patients with Fabry disease (Fabry), and patients with at least

moderate left ventricular hypertrophy (LVH). Four examples of the proposed classification of hypertrophy are shown in the four corners. CMR, cardiovascular magnetic resonance; CRT, cardiac resynchronization therapy; LVH, left ventricular hypertrophy; LVMi, left ventricular mass index; SD, standard deviations; GTi, global wall thickness index.

When the patients of the *survival cohort* (n = 1575), were classified using GTi and LVMi, the vast majority (78 %) were found to be normal, 6 % had concentric remodelling, 8 % had eccentric hypertrophy, and a similar number of 8 % had concentric hypertrophy. When comparing the four groups in terms of the composite end-point of death from all causes or HHF, the two groups of patients with hypertrophy did not differ (p = 0.77), and were therefore combined into a single hypertrophy group (16 % of all patients). This hypertrophy group had worse outcomes than both patients with concentric remodelling (p = 0.045), and patients classified as normal (p < 0.001). The patients with concentric remodelling also had a worse prognosis than the normal patients (p = 0.02). Kaplan-Meier curves for these three groups are shown below in Figure 16.

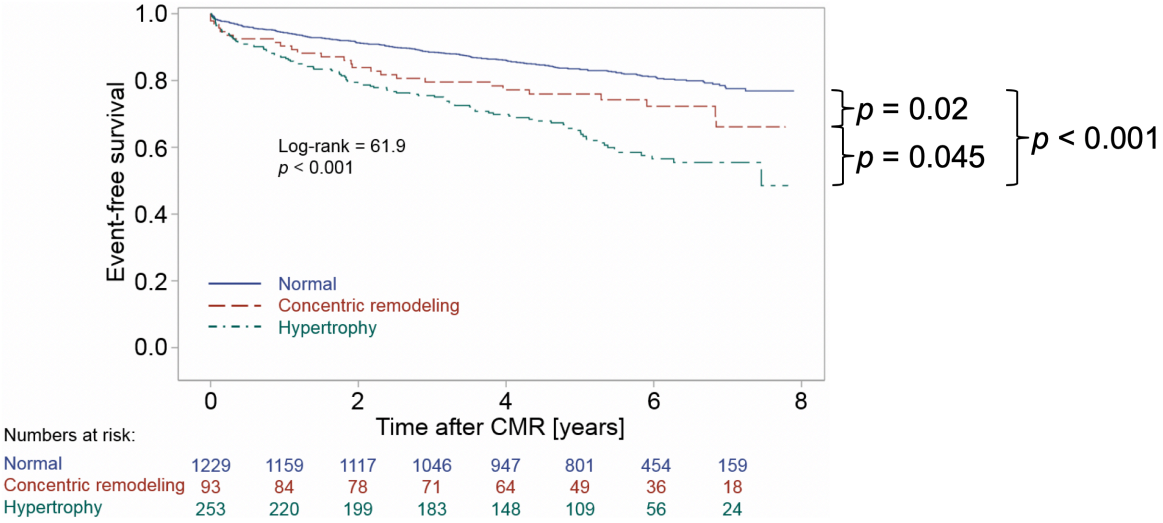

Figure 16. Kaplan-Meier curves for the survival cohort.
Kaplan-Meier curve for the patients of the *survival cohort* (n = 1575, follow-up time 5.4 [3.9–6.4] years) are shown with patients being classified as having either hypertrophy (increased LVMi regardless of GTi); concentric remodelling (normal LVMi, increased GTi); or being classified as normal (normal LVMi and GTi). The hypertrophic patients had a worse outcome compared to both the patients with concentric remodelling (p = 0.045) and the patients classified as being normal (p < 0.001). Patients with concentric remodelling also had worse prognosis compared to the normal group (p = 0.02). The limits for the GTi and LVMi were calculated from the healthy volunteers of the same study. CMR, cardiovascular magnetic resonance; GTi, global wall thickness indexed to body surface area; LVMi, left ventricular mass indexed to body surface area.

5.4 STUDY IV

A total of 63 patients were included in the study and the intracellular lifetime of water (τ) was found to be (median [interquartile range]) 78 [30–108] ms for normal patients (n = 17); 69 [13–107] ms for patients with concentric hypertrophy (n = 18); 73 [50–91]ms for patients with eccentric hypertrophy (n = 14), and 99 [63–175] ms for patients with concentric remodelling (n = 14). When comparing the results of the four groups, τ was found to be higher in patients with concentric remodelling than in patients with eccentric hypertrophy (p = 0.03), whereas no other group differed from any another group (p > 0.05), see Figure 3 of *Study IV*. Nine patients of the 63 (14 %) had a τ below 5 ms. Examples of two patients with very different τ are shown below in Figure 17.

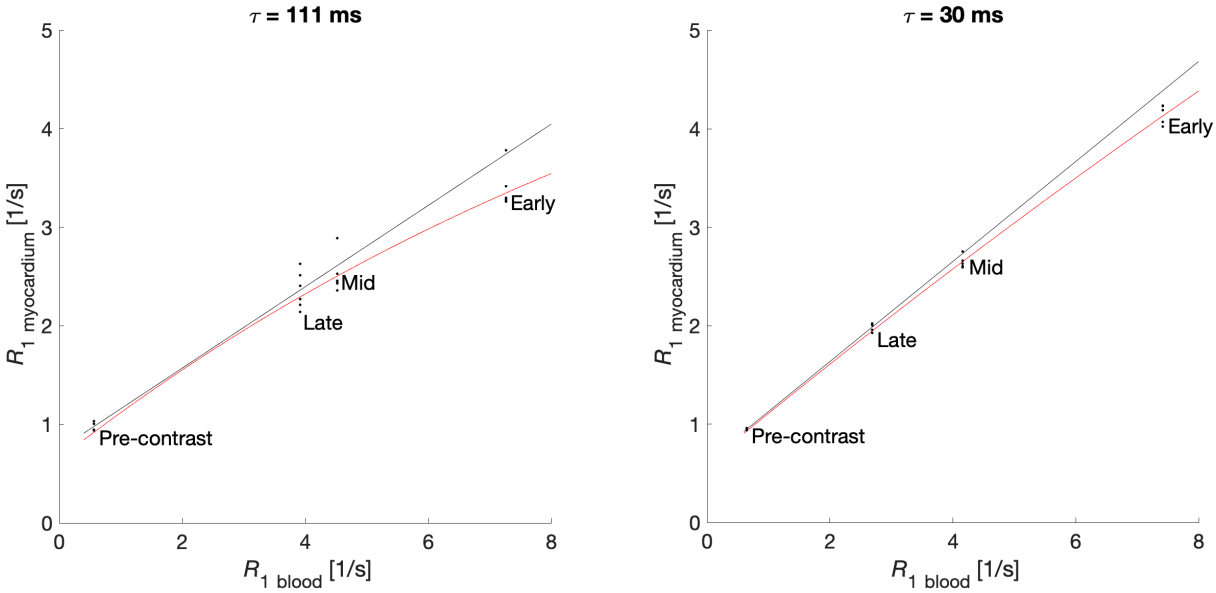

Figure 17. Examples of R_1 curves.
Examples of two patients with eccentric remodelling with R_1 in myocardium plotted versus R_1 in blood with the lowest R_1 values pre-contrast and the highest early post-contrast. The black line indicates the fast exchange (FX) model (Left: ECV_{FX} 28 %, Right: ECV_{FX} 27 %); the black dots show the results per myocardial segment; and the red curve shows the mean of the curve-fittings per segment for the slow exchange (SX) model, (Left: ECV_{SX} 32 %, τ 111 ms, Right: ECV_{SX} 27 %, τ 30 ms).

The slow exchange (SX) model used for calculating τ yielded higher ECV in all four groups compared to the commonly used fast exchange (FX) model (p < 0.01 for all groups), see Figure 4 of *Study IV*.

6 CONCLUSIONS

Study I: When detecting myocarditis using T_1 mapping, there was no clear benefit of performing early instead of late post-contrast imaging.

Study II: In this clinical population of 609 patients, 50 (8 %) had diffusely increased extracellular volume fraction that was not detected by other imaging techniques and 30 (60 %) of these patients did not have any focal findings. LV size was independently associated with increased ECV, whereas systolic dysfunction was independently associated with LGE.

Study III: Left ventricular mass indexed to body mass was the most prognostic measure for all-cause mortality and hospitalisation for heart failure in a large clinical population of 1575 patients. In the subset of patients with normal findings by cardiovascular magnetic resonance imaging who numbered 326, the new measure of global wall thickness (GT) was the most prognostic. This suggests that a combination of left ventricular mass and GT are the optimal measures for classifying left ventricular hypertrophy.

Study IV: Indirect measurement of cardiomyocyte size by contrast-enhanced cardiovascular magnetic resonance imaging is not reliable in a clinical setting with the described methods using the slow exchange model of transcytolemmal water exchange.

7 DISCUSSION

7.1 DETECTING MYOCARDITIS BY CMR

Study I (42) found no benefit of performing early post-contrast imaging (early gadolinium enhancement) when detecting acute myocarditis. On the other hand, focal abnormalities were more prominent late post-contrast as indicated by the greater difference in ECV between affected and unaffected segments at that time point, see Figure 8.

The early gadolinium enhancement (EGE) ratio was included in the so called *Lake Louise criteria* published in 2009 (37) and the EGE criterion was based upon four earlier studies (36,61–63). Since mapping techniques were not available at the time, T_1-weighted imaging was used. These images can show focal abnormalities well, but since they cannot detect abnormalities that affect the whole myocardium, skeletal muscle was chosen as a reference tissue.

An obvious problem with this method is that skeletal muscle can also be affected by a general inflammation. Indeed, this study found difference between skeletal muscle in myocarditis patients and in controls, see Figure 9. However, native T_1 and ECV of skeletal muscle was not higher in myocarditis patients as could be expected, rather, it was lower. The reasons for these findings are unclear but possible explanations could be dehydration or other unknown factors. Nevertheless, this illustrates the problem of using skeletal muscle as a reference tissue for myocardial imaging. By comparison, T_1 and ECV mapping provide measures in absolute units of measure.

When comparing remote myocardium in myocarditis patients to the healthy myocardium of controls we found that ECV did not differ either early or late post-contrast; that native T_1 was higher, but only slightly higher, in the remote myocardium in myocarditis patients compared to controls; and that global relative enhancement was higher in the remote myocardium of myocarditis patients compared to controls both early and late post-contrast. Since global relative enhancement uses skeletal muscle as a reference, these findings could be explained by the difference in skeletal muscle discussed above.

The original *Lake Louise criteria* (37) were updated in 2018 and no longer contain explicit recommendations for using EGE (64). The criteria now instead include oedema detected by T_2 weighted imaging or T_2 mapping, as well as abnormalities identified on either native T_1 maps, ECV maps or LGE images (64). Where the old criteria (37) stated that regional vasodilation in the myocardium caused enhancement early post-contrast, our findings do not support this theory, but rather indicate that enhancement is caused by an extracellular expansion and that the contrast agent is rapidly distributed in all extracellular space and does not give greater contrast enhancement early compared to late post-contrast. Although the 2018 criteria (37) do not include EGE, they do, however, mention early enhancement as a target for imaging when detecting myocarditis, and that it is unclear whether this is caused by hyperaemia or an extracellular expansion, where our findings suggest the latter.

7.2 PREVALENCE OF INCREASED ECV

The main finding of *Study II* was that 8 % of patients, in a clinical population consisting of patients with known or suspected heart disease, hade diffusely increased ECV in remote myocardium. Out of these patients, 60 % (5 % of all patients) had increased ECV without any focal findings. These patients represent a non-negligible part of all patients and an increased ECV, measured in myocardium that is free from focal LGE. Such ECV measurements have been found to be associated with adverse events including elevated mortality, and hospitalisation for cardiac reasons (27–31,57). These patients are important to identify at an early stage to provide the best possible treatment in order to mitigate adverse outcomes.

ECV in healthy volunteers was higher in females than in males, and female sex was also the strongest predictor of remote ECV in multivariate analysis. A previous study also found higher ECV in females than in males, but since ECV in males increased with age, the differences between the sexes disappeared for older patients (65). Different limits for females and males thus seem to be warranted, and perhaps also different limits for different age groups.

Increased ECV was more common in patients that had a pronounced dilatation of the left ventricle compared to patients without such dilatation. Previous studies have also shown that patients with dilated cardiomyopathy had higher ECV compared to controls (66–68). It has also been shown that ECV correlates well with the amount of collagen found in biopsy samples of these patients (66). There therefore seems to be a clear connection between diffuse myocardial fibrosis and dilatation, but the cause-effect relationship between the two remains unclear. By comparison, there was no difference in the prevalence of increased remote ECV in patients with or without a pronounced decrease in left ventricular systolic function.

In contrast, focal LGE findings were more common in patients with a pronounced decrease in left ventricular systolic function. Similarly, previous studies have found an inverse relationship between infarct size and left ventricular ejection faction in patients with myocardial infarction (69,70). These findings seem reasonable since focal lesions represent areas that do not contribute to the systolic function. However, the prevalence of focal LGE did not differ between patients with or without a pronounced dilatation.

7.3 GLOBAL WALL THICKNESS

The main finding of *Study III*, that a measure of the global mean wall thickness (GT) can be easily calculated from the end-diastolic volume (EDV) and mass of the left ventricle is arguably the most novel finding in this thesis.

In a large clinical cohort, left ventricular mass indexed (LVMi) to body surface area (BSA) was the most prognostic measure for the composite endpoint of all-cause mortality and hospitalisation for heart failure (HHF). The second most prognostic measure among all patients was GT indexed (GTi) to BSA. In the patients with normal findings, GT was more prognostic than all other measures, including both hypertension and age. GT (and therefore

GTi) also had a test-retest repeatability that was better than that for both LVM and EDV. In contrast to direct measurements of the wall thickness using either CMR or echocardiography, GT is less prone to sampling error and reflects the average wall thickness of the whole heart.

Previously proposed methods for characterising left ventricular hypertrophy have used measures including mass-to-volume ratio (71) and concentricity$^{0.67}$ (54,72). These measures are not immediately intuitive, and the latter methods also requires both concentricity$^{0.67}$, LV mass and LVEDV for characterizing hypertrophy. The method proposed in *Study IV* uses two measures, LVMi and GTi, which are both relatively intuitive.

Taken together, it seems reasonable to use GTi together with LVMi for characterising different forms of hypertrophy, as illustrated in Figure 15. When applying this methodology to the survival cohort, it was somewhat surprisingly found that there were no differences in adverse outcomes between eccentric and concentric hypertrophy, and these patients were therefore examined as one group. This lack of differences in outcomes between eccentric and concentric hypertrophy may have been in part related to a relatively smaller sample size for these subgroups. The combined hypertrophy group had a worse outcome compared to patients with concentric remodelling which in turn had worse outcomes than patients with normal mass and thickness.

The principle drawback of GT is that the EDV and LVM have to be determined by including papillary muscles and major trabeculations in the blood pool. For other ways of analysing EDV and LVM, a new equation for GT would need to be derived and verified.

7.4 MEASURING CARDIOMYOCYTE SIZE NON-INVASIVELY

The results from *Study IV* showed no difference in τ between different hypertrophy subgroups and controls despite defining the groups so as to maximise the chances of finding differences. That as many as 14 % the patients had intracellular lifetime of water (τ) values that were lower than 5 ms, which is not physiologically reasonable, indicates that the method is not robust and reliable enough to work for humans in a clinical setting despite working in mice.

Although mice and humans show many differences, myocyte size (15) and extracellular space, which is close to 25 % for both mice (9) and humans (16), are not among those differences. The dose of contrast agent in the previous work was 0.5 mmol/kg body weight (73,74) which is 2.5 times more than the of 0.2 mmol/kg of body weight was used for *Study IV*. A higher contrast dose would entail lower T_1 values and consequently higher R_1 values giving more certainty in curve-fitting. However, higher doses than 0.2 mmol/kg of body weigh are not recommended in humans. In the previous studies in mice, the contrast agent was also administered subcutaneously with step-wise increases. In *Study IV*, on the other hand, the contrast agent was administered intravenously as a bolus dose, and measurements were made for slowly decreasing rather than step-wise increasing contrast agent concentrations. This difference, as well as the lower dose of contrast agent, could have contributed to the results. A non-invasive method for measuring the size of the myocytes

could possibly be useful for diagnosing various heart diseases, including hypertrophy, and could also have prognostic implications.

8 ACKNOWLEDGEMENTS

I would first of all would like to thank my main supervisor **Martin Ugander** for his seemingly endless knowledge and ditto optimism. If you hadn't been such an incredibly positive person I would never have come this far.

Many thanks to my co-supervisors: **Andreas Sigfridsson** for his help and support over the years, not least by enlightening me regarding the inner works of MRI physics from an early start; and **Kenneth Caidahl** for his support during the years, not least in working behind the scenes to make sure that I and other PhD students have a good working environment.

I will always be grateful to **Peder Sörensson** for teaching me so much about CMR and for pushing me in the right direction. Thank you to **Jenny "Bagheera" Rasck** for her great sense of humour, for running the extra early MOLLI sequences needed for *Study I* and *Study IV* in particular, and for introducing me to *Dansbandskanalen*. Thank you also to **Karin Bouma**, **Márcia Guerra Tomé Ferreira**, **Sofie "Ulla-Bella" Olsson**, **Rebecca Almqvist** for their imaging skills and for their great company.

Thank you to **Eva Maret** for her clinical skills and sharp-eyed reading and to **Maria Eriksson** for her physiological insights and to both for their support in both my research and in my career. Many thanks to my mentor **Andreas Aly**.

I must of course also thank my research group, in particular: **Jannike Nickander** for her support and her herculean efforts in my early research project; **Maren "Gitaren" Maanja** for her great enthusiasm for expanding her knowledge on everything from ECV to trees, and for being a great travel companion; **Alexander Fyrdahl** for always taking time and helping out, with his vast knowledge in MRI physics and his vast patience with answering more or less intelligent question from people like me; **Björn "Wieschlan" Wieslander**; **Goran Abdula**; **Raquel Themudo**; **Simon Thalén**; **João "George" Afonso De Magalhães Peixoto E Génio Ramos**; **Mona Ahmed**; **Karen Holst**; **Elira Maksuti**; **Daniel "Grävenstein" Loewenstein**; and **Fredrik Fröjdh**. Thank you also to **Liya Vishnevskaya**; **Sara Demirtas**; **Sebastian Haby**; **Sammi Saers**; and **Andreas Fredholm**. I would also like to thank all members of *Dissonanskören* for the yearly singing performances.

Thank you to my **many co-authors**, in particular **Peter Kellman** for his technical support right from the start; **Erik Schelbert** for his expertise and hard work on prognostic analysis as well as for his advice on music; **Einar Heiberg** for programming skills that made *Study III* possible; **Rebecca Kozor** for her inputs and contributions to *Study III*; **Henrik Engblom** and **Katarina Steding Ehrenborg** for their early morning scanning.

I would also like to thank the people involved in my first project: **Pellina Janson**; A**nn-Christin Sandberg Nordqvist**; **Sandra Olsson**; **Anna-Lena Gustafsson**; **Roberto Vargas Paris**; **Yvonne Eriksson-Alm**; **Roberto Vargas Paris**; **Hamid Pesaran Behbahan**; with a special thanks to **Marjo Salokivi** for making me feel very welcome at the radiology department.

Thank you to all the lovely people at *Fysiologkliniken* for making me feel so welcome, in particular **Pia Ullström**, **Lena Forsberg**, **Jonas Jenner**, **Joakim Norderfeldt**, **Carola Steenberg**, **Jan Engvall**, **Nina Samadi**, **Anna Asp**, **Helena Wallin**, Monsieur **Patrik Norgren**, and last, but certainly not least, **Ingrid Berggren** who came to the clinic at the same time as I, and who has been a good friend ever since.

Thank you to **Jan-Erik Kaare** and **Ann-Britt Wikström** at the Department for molecular medicine and surgery for their enduring support.

I would also like to thank the lovely colleagues and friendly patients at *Vårby Vårdcentral*, in particular my supervisor **Ingela**, but also **Jan**, **Liz** , **Suzana**, **Elisabet**, **Maria**, **Aygun**, **Johanna** and all others; as well as my dear intern colleagues at *Huddinge*: **Cecilia Fahlén Bergh**, **Max Grönholdt Klein**, **Malin Sveijer, Erik Larsson**, and **Pauline Cewe**.

Thank you to **all of my friends** who knowingly or unknowingly have supported me over the years, in particular **Mattias Eriksson** & *la famiglia*; **Alexander Björkqvist**; **Jonna "Kitty" Eriksson**; **Susanna** & **Clas Torehammar**; **Magnus** "**Majken" Linderoth**; **Andreas Eriksson**; **Elin** & **Pelle**; **Siri Sandqvist**; **Stina Slettenmark**; **Teddie** "**Ale" Aleberg; Johanna Classon**; **Moa Stenudd**; **Evy**, **Lia** and the rest of *Brunchgänget*; **Johanna**, **Susanna**, **Sandra** and the rest of *Adventsgänget*; **Henrik**, **Roberth**, **Philip**, **Ola** and the other friendly people at DBD and PB; and all the lovely people of *Blåslaget*: **Ylva**, **Ulf**, **Nadine**, **Duvis**, madame **Jacquet**, **Louise**, **Gunnar**, **Mikaela**, **Karin**, **Anders** & **Marina**, **Schtina**, **Klur**, **Flygarn**, **Angelica**, **Styrman**, **Falcon**, **Moe**, **Stefan**, **Mamma Mu**, **Kråkan**, **Skatan**, **Hoffe**, **Torsken**, **påläggs-Pär**, **Mallis**, **Power**, **Rädisa**, **Reenis**, **Curry**, **Körvel**, **Wää**, **Keynå**, **Jäger**, **Häger**, **Skreckis**, **Bronner**, **Twajlajt**, **Sölve**, **sofie sofie**, **Gäddan**, **Lovisa**, **Baewatch**, **Strömming**, **Oda**, **Ab-Gr**, **Dukat**, **Kvarten**, **Kalle**, **Mackan**, **Kardemumma**, **Guldeböj**, **Niten**, **Hagman**, **Nelson**, **Schlager**, etc.

Finally, a very heartfelt thanks to my family for their kindness and support from the very start: **Anita**, **Ingemar**, **Maria**, and, **Fredrik**; and also to my extended family including **Mikael**, **Elisabet**, **Peter**, **Viktor**, **Axel**, **Caroline**, as well as **Quarolin**.

9 REFERENCES

1. Hanson LG. Is quantum mechanics necessary for understanding magnetic resonance? Concepts Magn Reson Part A. 2008;32A(5):329–340.

2. Look D, Locker D. Nuclear spin-lattice relaxation measurements by tone-burst modulation. Phys Rev Lett. 1968;20(18):987–989.

3. Look D, Locker D. Time Saving in Measurement of NMR and EPR Relaxation Times. Rev Sci Instrum. 1970;41(2):250–251.

4. Messroghli DR, Radjenovic A, Kozerke S, Higgins DM, Sivananthan MU, Ridgway JP. Modified Look-Locker inversion recovery (MOLLI) for high-resolution T1 mapping of the heart. Magn Reson Med. 2004;52(1):141–146.

5. Sparrow P, Messroghli DR, Reid S, Ridgway JP, Bainbridge G, Sivananthan MU. Myocardial T1 mapping for detection of left ventricular myocardial fibrosis in chronic aortic regurgitation: pilot study. AJR Am J Roentgenol. 2006;187(6):W630-5.

6. Deichmann R, Haase A. Quantification of T1 values by SNAPSHOT-FLASH NMR imaging. J Magn Reson. 1992;96(3):608–612.

7. Ugander M, Oki AJ, Hsu L-Y, et al. Extracellular volume imaging by magnetic resonance imaging provides insights into overt and sub-clinical myocardial pathology. Eur Heart J. 2012;33(10):1268–1278.

8. Salerno M, Janardhanan R, Jiji RS, et al. Comparison of methods for determining the partition coefficient of gadolinium in the myocardium using T1 mapping. J Magn Reson Imaging. 2013;38(1):217–224.

9. Kellman P, Wilson JR, Xue H, Ugander M, Arai AE. Extracellular volume fraction mapping in the myocardium, part 1: evaluation of an automated method. J Cardiovasc Magn Reson. 2012;14(1):63.

10. Piechnik SK, Ferreira VM, Dall'Armellina E, et al. Shortened Modified Look-Locker Inversion recovery (ShMOLLI) for clinical myocardial T1-mapping at 1.5 and 3 T within a 9 heartbeat breathhold. J Cardiovasc Magn Reson. BioMed Central Ltd; 2010;12(1):69.

11. Chow K, Flewitt JA, Green JD, Pagano JJ, Friedrich MG, Thompson RB. Saturation recovery single-shot acquisition (SASHA) for myocardial T_1 mapping. Magn Reson Med. 2014;71(6):2082–2095.

12. Kellman P, Hansen MS. T1-mapping in the heart: accuracy and precision. J Cardiovasc Magn Reson. Journal of Cardiovascular Magnetic Resonance; 2014;16(1):2.

13. Arheden H, Saeed M, Higgins CB, et al. Measurement of the Distribution Volume of Gadopentetate Dimeglumine at Echo-planar MR Imaging to Quantify Myocardial Infarction: Comparison with 99m Tc-DTPA Autoradiography in Rats. Radiology. 1999;211(3):698–708.

14. Kellman P, Wilson JR, Xue H, Ugander M, Arai AE. Extracellular volume fraction mapping in the myocardium, part 1: evaluation of an automated method. J Cardiovasc Magn Reson. 2012;14(1):63.

15. Caravan P. Strategies for increasing the sensitivity of gadolinium based MRI contrast agents. Chem Soc Rev. 2006;35(6):512–523.

16. Rogosnitzky M, Branch S. Gadolinium-based contrast agent toxicity: a review of known and proposed mechanisms. BioMetals. Springer Netherlands; 2016;29(3):365–376.

17. Fraum TJ, Ludwig DR, Bashir MR, Fowler KJ. Gadolinium-based contrast agents: A comprehensive risk assessment. J Magn Reson Imaging. 2017;46(2):338–353.

18. Grobner T. Gadolinium - A specific trigger for the development of nephrogenic fibrosing dermopathy and nephrogenic systemic fibrosis? Nephrol Dial Transplant. 2006;21(4):1104–1108.

19. McNamara MT, Higgins CB, Ehman RL, Revel D, Sievers R, Brasch RC. Acute myocardial ischemia: Magnetic resonance contrast enhancement with gadolinium-DTPA. Radiology. 1984;153(1):157–163.

20. Kim RJ, Fieno DS, Parrish TB, et al. Relationship of MRI Delayed Contrast Enhancement to Irreversible Injury, Infarct Age, and Contractile Function. Circulation. 1999;100(19):1992–2002.

21. Mahrholdt H, Wagner A, Judd RM, Sechtem U, Kim RJ. Delayed enhancement cardiovascular magnetic resonance assessment of non-ischaemic cardiomyopathies. Eur Heart J. 2005;26(15):1461–1474.

22. Ordovas KG, Higgins CB. Delayed Contrast Enhancement on MR Images of Myocardium: Past, Present, Future. Radiology. 2011;261(2):358–374.

23. Kellman P, Arai AE, McVeigh ER, Aletras AH. Phase-sensitive inversion recovery for detecting myocardial infarction using gadolinium-delayed hyperenhancement. Magn Reson Med. 2002;47(2):372–383.

24. Abdula G, Nickander J, Sörensson P, et al. Synthetic late gadolinium enhancement cardiac magnetic resonance for diagnosing myocardial scar. Scand Cardiovasc J. Informa UK Limited, trading as Taylor & Francis Group; 2018;52(3):127–132.

25. Gazoti Debessa CR, Mesiano Maifrino LB, Rodrigues de Souza R. Age related changes of the collagen network of the human heart. Mech Ageing Dev. 2001;122(10):1049–1058.

26. Flett AS, Hayward MP, Ashworth MT, et al. Equilibrium contrast cardiovascular magnetic resonance for the measurement of diffuse myocardial fibrosis: preliminary validation in humans. Circulation. 2010;122(2):138–144.

27. Kammerlander AA, Marzluf BA, Zotter-Tufaro C, et al. T1 Mapping by CMR Imaging. JACC Cardiovasc Imaging. 2016;9(1):14–23.

28. Treibel TA, Fontana M, Maestrini V, et al. Automatic Measurement of the Myocardial Interstitium. JACC Cardiovasc Imaging. 2016;9(1):54–63.

29. Wong TC, Piehler K, Meier CG, et al. Association between extracellular matrix expansion quantified by cardiovascular magnetic resonance and short-term mortality. Circulation. 2012;126(10):1206–1216.

30. Wong TC, Piehler KM, Kang IA, et al. Myocardial extracellular volume fraction

quantified by cardiovascular magnetic resonance is increased in diabetes and associated with mortality and incident heart failure admission. Eur Heart J. 2014;35(10):657–664.

31. Schelbert EB, Piehler KM, Zareba KM, et al. Myocardial fibrosis quantified by extracellular volume is associated with subsequent hospitalization for heart failure, death, or both across the spectrum of ejection fraction and heart failure stage. J Am Heart Assoc. 2015;4(12).

32. Kawai C. From Myocarditis to Cardiomyopathy: Mechanisms of Inflammation and Cell Death : Learning From the Past for the Future. Circulation. 1999;99(8):1091–1100.

33. Blauwet LA, Cooper LT. Myocarditis. Prog Cardiovasc Dis. 2010;52(4):274–288.

34. Butts RJ, Boyle GJ, Deshpande SR, et al. Characteristics of Clinically Diagnosed Pediatric Myocarditis in a Contemporary Multi-Center Cohort. Pediatr Cardiol. Springer US; 2017;38(6):1175–1182.

35. Aretz HT, Billingham ME, Edwards WD, et al. Myocarditis: a histopathologic definition and classification. Am J Cardiovasc Pathol. 1987;1(1):3–14.

36. Friedrich MG, Strohm O, Schulz-Menger J, Marciniak H, Luft FC, Dietz R. Contrast Media Enhanced Magnetic Resonance Imaging Visualizes Myocardial Changes in the Course of Viral Myocarditis. Circulation. 1998;97(18):1802–1809.

37. Friedrich MG, Sechtem U, Schulz-Menger J, et al. Cardiovascular Magnetic Resonance in Myocarditis: A JACC White Paper. J Am Coll Cardiol. American College of Cardiology Foundation; 2009;53(17):1475–1487.

38. Miller DD, Holmvang G, Gill JB, et al. MRI detection of myocardial perfusion changes by gadolinium-DTPA infusion during dipyridamole hyperemia. Magn Reson Med. 1989;10(2):246–255.

39. Paajanen H, Brasch RC, Schmiedl U, Ogan M. Magnetic resonance imaging of local soft tissue inflammation using gadolinium-DTPA. Acta radiol. 1987;28(1):79–83.

40. Chu GCW, Flewitt JA, Mikami Y, Vermes E, Friedrich MG. Assessment of acute myocarditis by cardiovascular MR: Diagnostic performance of shortened protocols. Int J Cardiovasc Imaging. 2013;29(5):1077–1083.

41. Luetkens JA, Doerner J, Thomas DK, et al. Acute Myocarditis: Multiparametric Cardiac MR Imaging. Radiology. 2014;273(2):383–392.

42. Lundin M, Sörensson P, Vishnevskaya L, et al. Detection of myocarditis using T1 and ECV mapping is not improved by early compared to late post-contrast imaging. Clin Physiol Funct Imaging. 2019;384–392.

43. Grothues F, Smith GC, Moon JCC, et al. Comparison of interstudy reproducibility of cardiovascular magnetic resonance with two-dimensional echocardiography in normal subjects and in patients with heart failure or left ventricular hypertrophy. Am J Cardiol. 2002;90(1):29–34.

44. Grant C, Greene DG, Bunnell IL. Left Ventricular Enlargement and Hypertrophy. A Clinical and Angiocardiographic Study. Am J Med. 1965;39(6):895–904.

45. Verdecchia P, Schillaci G, Borgioni C, et al. Adverse prognostic significance of concentric remodeling of the left ventricle in hypertensive patients with normal left ventricular mass. J Am Coll Cardiol. 1995;25(4):871–878.

46. Levy D, Garrison RJ, Savage DD, Kannel WB, Castelli WP. Prognostic implications of echocardiographically determined left ventricular mass in the Framingham Heart Study. N Engl J Med. 1990;322(22):1561–1566.

47. Pelliccia A, Maron BJ. Outer limits of the athlete's heart, the effect of gender and relevance to the differential diagnosis with primary cardiac disease. Cardiol Clin. 1997;15(3):381–396.

48. Fagard R. Athlete's heart. Heart. 2003;89:1455–1461.

49. Zamorano JL, Anastasakis A, Borger MA, et al. 2014 ESC guidelines on diagnosis and management of hypertrophic cardiomyopathy: The task force for the diagnosis and management of hypertrophic cardiomyopathy of the European Society of Cardiology (ESC). Eur Heart J. 2014;35(39):2733–2779.

50. Maron BJ, Haas TS, Ahluwalia A, Murphy CJ, Garberich RF. Demographics and Epidemiology of Sudden Deaths in Young Competitive Athletes: From the United States National Registry. Am J Med. Elsevier Inc; 2016;129(11):1170–1177.

51. Maron BJ. Distinguishing hypertrophic cardiomyopathy from athlete's heart: a clinical problem of increasing magnitude and significance. Heart. 2005;91(11):1380–1382.

52. Ganau A, Devereux RB, Roman MJ, et al. Patterns of left ventricular hypertrophy and geometric remodeling in essential hypertension. J Am Coll Cardiol. 1992;19(7):1550–1558.

53. Gaasch WH, Zile MR. Left ventricular structural remodeling in health and disease: With special emphasis on volume, mass, and geometry. J. Am. Coll. Cardiol. Elsevier Inc.; 2011. p. 1733–1740.

54. Khouri MG, Peshock RM, Ayers CR, De Lemos JA, Drazner MH. A 4-tiered classification of left ventricular hypertrophy based on Left ventricular geometry the dallas Heart study. Circ Cardiovasc Imaging. 2010;3(2):164–171.

55. Mascherbauer J, Marzluf BA, Tufaro C, et al. Cardiac Magnetic Resonance Postcontrast T1 Time Is Associated With Outcome in Patients With Heart Failure and Preserved Ejection Fraction. Circ Cardiovasc Imaging. 2013;6(6):1056–1065.

56. Nickander J, Themudo R, Thalén S, et al. The relative contributions of myocardial perfusion, blood volume and extracellular volume to native T1 and native T2 at rest and during adenosine stress in normal physiology. J Cardiovasc Magn Reson. Journal of Cardiovascular Magnetic Resonance; 2019;21(1):1–10.

57. Treibel TA, Fridman Y, Bering P, et al. Extracellular Volume Associates With Outcomes More Strongly Than Native or Post-Contrast Myocardial T1. JACC Cardiovasc Imaging. 2020;13(1 Pt 1):44–54.

58. Cerqueira MD, Weissman NJ, Dilsizian V, et al. Standardized Myocardial Segmentation and Nomenclature for Tomographic Imaging of the Heart. Circulation. 2002;105(4):539–542.

59. Mosteller RD. Simplified Calculation of Body-Surface Area. N Engl J Med.

1987;317(17):1098–1098.

60. Landis CS, Li X, Telang FW, et al. Equilibrium Transcytolemmal Water-Exchange Kinetics in Skeletal Muscle In Vivo. Magn Reson Med. 1999;478:467–478.

61. Laissy JP, Messin B, Varenne O, et al. MRI of acute myocarditis: A comprehensive approach based on various imaging sequences. Chest. 2002;122(5):1638–1648.

62. Abdel-Aty H, Boyé P, Zagrosek A, et al. Diagnostic performance of cardiovascular magnetic resonance in patients with suspected acute myocarditis: Comparison of different approaches. J Am Coll Cardiol. 2005;45(11):1815–1822.

63. Gutberlet M, Spors B, Thoma T, et al. Suspected Chronic Myocarditis at Cardiac MR: Diagnostic Accuracy and Association with Immunohistologically Detected Inflammation and Viral Persistence 1. Radiology. 2008;246(2):401–409.

64. Ferreira VM, Schulz-Menger J, Holmvang G, et al. Cardiovascular Magnetic Resonance in Nonischemic Myocardial Inflammation: Expert Recommendations. J Am Coll Cardiol. 2018;72(24):3158–3176.

65. Liu C-Y, Liu Y-C, Wu C, et al. Evaluation of Age-Related Interstitial Myocardial Fibrosis With Cardiac Magnetic Resonance Contrast-Enhanced T 1 Mapping. J Am Coll Cardiol. 2013;62(14):1280–1287.

66. aus dem Siepen F, Buss SJ, Messroghli D, et al. T1 mapping in dilated cardiomyopathy with cardiac magnetic resonance: quantification of diffuse myocardial fibrosis and comparison with endomyocardial biopsy. Eur Heart J Cardiovasc Imaging. 2015;16(2):210–216.

67. Hong YJ, Park CH, Kim YJ, et al. Extracellular volume fraction in dilated cardiomyopathy patients without obvious late gadolinium enhancement: comparison with healthy control subjects. Int J Cardiovasc Imaging. Springer Netherlands; 2015;31 Suppl 1:115–122.

68. Jerosch-Herold M, Sheridan DC, Kushner JD, et al. Cardiac magnetic resonance imaging of myocardial contrast uptake and blood flow in patients affected with idiopathic or familial dilated cardiomyopathy. Am J Physiol Heart Circ Physiol. 2008;295(3):H1234–H1242.

69. Wu E, Ortiz JT, Tejedor P, et al. Infarct size by contrast enhanced cardiac magnetic resonance is a stronger predictor of outcomes than left ventricular ejection fraction or end-systolic volume index: prospective cohort study. Heart. 2008;94(6):730–736.

70. Ugander M, Ekmehag B, Arheden H. The relationship between left ventricular ejection fraction and infarct size assessed by MRI. Scand Cardiovasc J. 2008;42(2):137–145.

71. Rosen BD, Edvardsen T, Lai S, et al. Left ventricular concentric remodeling is associated with decreased global and regional systolic function: the Multi-Ethnic Study of Atherosclerosis. Circulation. 2005;112(7):984–991.

72. Bang CN, Gerdts E, Aurigemma GP, et al. Systolic left ventricular function according to left ventricular concentricity and dilatation in hypertensive patients: The Losartan Intervention for Endpoint reduction in hypertension study. J Hypertens. 2013;31(10):2060–2068.

73. Coelho-Filho OR, Shah R V., Mitchell R, et al. Quantification of cardiomyocyte

hypertrophy by cardiac magnetic resonance: Implications for early cardiac remodeling. Circulation. 2013;128(11):1225–1233.

74. Coelho-Filho OR, Mongeon FP, Mitchell R, et al. Role of transcytolemmal water-exchange in magnetic resonance measurements of diffuse myocardial fibrosis in hypertensive heart disease. Circ Cardiovasc Imaging. 2013;6(1):134–141.